

Minerva Access is the Institutional Repository of The University of Melbourne

Author/s:

Sampaio, NG;Emery, SJ;Garnham, AL;Tan, QY;Sisquella, X;Pimentel, MA;Jex, AR;Regev-Rudzki, N;Schofield, L;Eriksson, EM

Title:

Extracellular vesicles from early stage Plasmodium falciparum-infected red blood cells contain PfEMP1 and induce transcriptional changes in human monocytes

Date:

2018-05-01

Citation:

Sampaio, N. G., Emery, S. J., Garnham, A. L., Tan, Q. Y., Sisquella, X., Pimentel, M. A., Jex, A. R., Regev-Rudzki, N., Schofield, L. & Eriksson, E. M. (2018). Extracellular vesicles from early stage Plasmodium falciparum-infected red blood cells contain PfEMP1 and induce transcriptional changes in human monocytes. *Cellular Microbiology*, 20 (5), <https://doi.org/10.1111/cmi.12822>.

Persistent Link:

<https://hdl.handle.net/11343/283538>

1 Extracellular vesicles from early-stage *P. falciparum*-infected red blood cells contain
2 PfEMP1 and induce transcriptional changes in human monocytes

3 Running title: *P. falciparum* vesicles have PfEMP1 and affect monocytes

4
5 Natália G. Sampaio^{a,b}, Samantha Emery^{a,b}, Alexandra Garnham^{b,c}, Qiao Y. Tan^{a,b},
6 Xavier Sisquella^{b,d}, Matthew A. Pimentel^{b,d}, Neta Regev-Rudzki^{b,d}, Louis Schofield^{a,e},
7 Emily M. Eriksson^{a,b}

8 ^a Population Health and Immunity Division, Walter and Eliza Hall Institute of Medical
9 Research, Parkville, Victoria, Australia

10 ^b Department of Medical Biology, University of Melbourne, Parkville, Victoria,
11 Australia

12 ^c Bioinformatics Division, Walter and Eliza Hall Institute of Medical Research,
13 Parkville, Victoria, Australia

14 ^d Infection and Immunity Division, Walter and Eliza Hall Institute of Medical
15 Research, Parkville, Victoria, Australia

16 ^e Australian Institute of Tropical Health and Medicine, James Cook University,
17 Townsville, Queensland, Australia

18
19 Corresponding author:

20 Emily M. Eriksson

21 The Walter and Eliza Hall Institute of Medical Research

22 **This is the author manuscript accepted for publication and has undergone full peer review but
1G Royal Parade, VIC 3052 Australia**

23 **has not been through the copyediting, typesetting, pagination and proofreading process, which
may lead to differences between this version and the Version of Record. Please cite this article
as doi: 10.1111/cmi.12822**
Tel: +61 3 93452462, Fax: +61 3 93470852, email: eriksson@wehi.edu.au

24

25 Current affiliations:

26 NGS - Medical Research Council Human Immunology Unit, Radcliffe Department of

27 Medicine, Medical Research Council Weatherall Institute of Molecular Medicine,

28 University of Oxford, Oxford, UK

29

30 NRR - Department of Biomolecular Sciences, Weizmann Institute of Science,

31 Rehovot, Israel

32

33

Author Manuscript

34 **Summary**

35 Pathogens can release extracellular vesicles (EVs) for cell-cell communication and
36 host modulation. EVs from *Plasmodium falciparum*, the deadliest malaria parasite
37 species, can transfer drug resistance genes between parasites. EVs from late-stage
38 parasite-infected RBC (iRBC-EVs) are immunostimulatory and affect endothelial cell
39 permeability, but little is known about EVs from early-stage iRBC. We detected the
40 parasite virulence factor PfEMP1, which is responsible for iRBC adherence and a
41 major contributor to disease severity, in EVs only up to 12 hours-post RBC invasion.
42 Furthermore, using PfEMP1 transport knock-out parasites, we determined that EVs
43 originated from inside the iRBC rather than the iRBC surface. Proteomic analysis
44 detected 101 parasite and 178 human proteins in iRBC-EVs. Primary human
45 monocytes stimulated with iRBC-EVs released low levels of inflammatory cytokines,
46 and showed transcriptomic changes. Stimulation with iRBC-EVs from PfEMP1
47 knock-out parasites induced more gene expression changes, and affected pathways
48 involved in defense response, stress response, and response to cytokines,
49 suggesting a novel function of PfEMP1 when present in EVs. We show for the first
50 time the presence of PfEMP1 in early-stage *P. falciparum* iRBC-EVs, and the effects
51 of these EVs on primary human monocytes, uncovering a new mechanism of
52 potential parasite pathogenesis and host interaction.

53

54

55 Introduction

56 The apicomplexan parasite *Plasmodium falciparum* caused 99% of the
57 estimated 429,000 malaria deaths in 2015, predominantly affecting children in sub-
58 Saharan Africa (WHO Malaria Report 2016). Mortality arises from severe disease
59 complications such as anemia, metabolic acidosis, and cerebral malaria (White et
60 al., 2014). *P. falciparum* invades red blood cells (RBC) and progresses through
61 several distinct stages over a 48 hour asexual life cycle. After invasion, the parasite
62 is surrounded by the parasitophorous vacuole, and is visualized as a ring in
63 microscopy, hence named 'ring stage'. As the parasite develops inside the RBC, it
64 enters the trophozoite stage, and then matures into a schizont prior to RBC rupture
65 and parasite egress in the form of many invasive merozoites.

66 As the parasite progresses through the intraerythrocytic life cycle, the host cell
67 is significantly altered. These changes are caused by the production and export of
68 parasite proteins, of which many are inserted into the RBC plasma membrane; and
69 by the introduction of parasite organelles, such as the Maurer's Clefts, into the RBC
70 cytoplasm (Maier, Cooke, Cowman, & Tilley, 2009). A key parasite protein at the
71 RBC surface is *Plasmodium falciparum* erythrocyte membrane protein 1 (PfEMP1).
72 PfEMP1 binds to host cell surface molecules such as ICAM-1, CD36 and CSA, and
73 causes iRBC sequestration in blood vessels and organs in order to avoid destruction
74 in the spleen (Baruch, Gormely, Ma, Howard, & Pasloske, 1996; Reeder et al., 1999;
75 Schofield & Grau, 2005). This adherence is a major contributor to *P. falciparum*
76 pathogenesis, and can lead to particularly severe complications when sequestration
77 occurs in blood vessels of the brain (Jensen et al., 2004; Tembo et al., 2014).
78 Furthermore, PfEMP1 can dampen cytokine release from NK cells, $\gamma\delta$ T cells

79 (D’Ombrain et al., 2007), and monocytes (Sampaio et al., 2017). PfEMP1 is
80 produced early in the intraerythrocytic life cycle, already detectable in the parasite 8
81 hours post-invasion, and is shuttled through Maurer’s Clefts to appear at the iRBC
82 surface from 16 hours post-invasion (Kriek et al., 2003; McMillan et al., 2013). As a
83 result, cytoadherence of the iRBC occurs when parasites are in the trophozoite
84 stage, but early ring-stage parasites remain in circulation.

85 There have been increasing investigations into the role of extracellular
86 vesicles (EVs) in malaria biology and pathogenesis (recently reviewed here
87 (Sampaio, Cheng, & Eriksson, 2017)). EVs are bi-lipid membrane vesicles that are
88 released from cells, either by budding from the plasma membrane or by generation
89 and release of intravesicular bodies. They generally contain proteins and nucleic
90 acids, and can fuse or be endocytosed by other cells. Mouse models of *Plasmodium*
91 infection showed that parasite-derived EVs can induce an immune response (Couper
92 et al., 2010; Martin-Jaular, Nakayasu, Ferrer, Almeida, & Del Portillo, 2011).
93 Similarly, EVs from late-stage trophozoite/schizonts, can induce an inflammatory
94 response from human monocytes/macrophages (Mantel et al., 2013) and can
95 modulate epithelial cell gene expression and barrier properties (Mantel et al., 2016).
96 Furthermore, *P. falciparum* iRBC-derived EVs allow cell-cell communication between
97 parasites, and EVs from ring-stage iRBC were particularly efficient at parasite-to-
98 parasite gene transfer (Mantel et al., 2013; Regev-Rudzki et al., 2013). However, the
99 study of EVs from the early ring-stage of the asexual lifecycle has been limited.
100 Therefore, we aimed to investigate this population of vesicles and examine the effect
101 of EVs on host innate immune cells.

102 We hypothesized that ring-stage iRBC would release vesicles with unique
103 characteristics, and that these could stimulate host monocytes. We analysed EVs
104 from iRBC at different life stages, and found that the protein content of EVs changed
105 over time. Intriguingly, we discovered that the key *P. falciparum* virulence factor
106 PfEMP1 was present only in EVs from early ring-stage parasites, many hours before
107 PfEMP1 appearance on the iRBC surface, providing a means of the parasite to
108 disseminate PfEMP1 early in infection. Furthermore, these ring-stage EVs induce
109 low level cytokine responses from human primary monocytes, while altering the
110 cellular transcriptome. The EV effects on gene expression were partially PfEMP1-
111 dependent, suggesting a role for EV-delivered PfEMP1 in modulating the host
112 immune response to infection.

113

114 **Results**

115 **Extracellular vesicles from early-stage iRBC contain the virulence factor** 116 **PfEMP1**

117 To investigate the potential changes in the protein content of EVs released
118 during the parasite life cycle, vesicles were obtained from iRBC (iRBC-EVs) at
119 different stages of maturity. Wild type CS2 iRBC were tightly synchronised to a 4-
120 hour window, and vesicles were isolated in 12 hour increments, i.e. at 12, 24, 36 and
121 48 hours post-invasion, representing ring, early trophozoite, late trophozoite and
122 schizont stages (Figure 1A). The iRBC-EVs from the four different stages were
123 analysed by Western blot for the presence of *P. falciparum* proteins PfEMP1,
124 Plasmeprin V, aldolase, and actin depolymerisation factor (ADF1). PfEMP1 is a key

125 virulence factor, and EVs derived from ring stage iRBC contained PfEMP1, whereas
126 PfEMP1 was absent in EVs after 12 hours (Figure 1B). Notably, PfEMP1 is reported
127 to appear on the iRBC surface from 16 hours post-invasion and peak at 36 hours
128 post-invasion (Kriek et al., 2003), and we confirmed this timing with iRBC lysates at
129 the indicated 12 hour intervals (Figure 1C). PfEMP1 is therefore present in iRBC-
130 EVs significantly earlier than it's expression on the iRBC surface. The levels of other
131 parasite proteins in iRBC-EVs also varied at different life-stages. Parasite aldolase,
132 an actin-binding protein involved in parasite invasion and motility (Diaz et al., 2014),
133 was found at high levels in both ring stage and schizont-stage iRBC-EVs, whereas
134 parasite ADF1, another actin-binding protein (Wong et al., 2014), was abundant in
135 iRBC-EVs from the schizont-stage (Figure 1B). SR1 is a RBC protein and known
136 marker of erythrocyte-derived vesicles (Salzer, Hinterdorfer, Hunger, Borken, &
137 Prohaska, 2002), and was used to demonstrate equivalent loading of all samples.
138 Thus, we find that parasite proteins in iRBC-EVs vary throughout the parasite life
139 cycle, and that PfEMP1 is present only in EVs from early ring-stage iRBC.

140 **PfEMP1 presence in extracellular vesicles is independent of transport proteins**
141 **SBP1 and PTP1**

142 The transport of PfEMP1 from the parasite within the parasitophorous vacuole
143 to the iRBC plasma membrane is a regulated process involving many parasite
144 proteins (Maier et al., 2009). Genetic ablation of key proteins in this transport
145 pathway, such as skeletal binding protein 1 (SBP1), or PfEMP1 transport protein 1
146 and 2 (PTP1 and PTP2), results in PfEMP1 being expressed but localized in the
147 parasite or parasitophorous vacuole rather than the iRBC plasma membrane (Cooke
148 et al., 2006; Maier et al., 2007; Maier et al., 2008). EVs from CS2-SBP1-KO, CS2-

149 PTP1-KO and CS2-PTP2-KO iRBC were analysed for the presence of PfEMP1.
150 iRBC-EVs from both CS2-SBP1-KO and CS2-PTP1-KO still contained PfEMP1,
151 whereas PfEMP1 expression was negligible both CS2-PTP2-KO iRBC and iRBC-
152 EVs (Figure 2A). However, parasite aldolase and ADF1 were still detected in EVs
153 from CS2-PTP2-KO iRBC. Thus, SBP1 and PTP1 are not required for PfEMP1
154 incorporation into EVs, or EV release from iRBC. This data suggests that the EVs
155 originate from the intracellular parasite rather than budding from the RBC
156 membrane, as vesicles budding from the membrane of CS2-SBP1-KO or CS2-
157 PTP1-KO iRBC would not contain PfEMP1.

158 **Proteomic analysis of iRBC-EVs allowed quantitative discovery of parasite and** 159 **human proteins in EVs**

160 In order to investigate the potential downstream effects of PfEMP1 in iRBC-
161 EVs, we first performed an in-depth analysis of the proteins present in EVs from ring-
162 stage wild type 3D7 (3D7-WT) and the 3D7-UpsC^R PfEMP1 knock-out parasite
163 strain. The 3D7-UpsC parasite contains the *hdhfr* gene, which confers resistance to
164 WR99210, downstream of the UpsC PfEMP1 promoter (Voss et al., 2006). Due to
165 the allelic exclusivity of PfEMP1 expression, where only one PfEMP1-encoding gene
166 is expressed at a time, the 3D7-UpsC^R does not express PfEMP1 in the presence of
167 WR99210. Western blot analysis confirmed that PfEMP1 was present in iRBC-EVs
168 from ring-stage 3D7-WT and absent in those from 3D7-UpsC^R (Figure 2B). To
169 determine if proteins other than PfEMP1 were also differentially expressed in the
170 iRBC-EVs from 3D7-UpsC^R compared to 3D7-WT, label-free, quantitative
171 proteomics of EV proteins was performed. To obtain highly purified iRBC-EVs,
172 culture supernatant was fractionated by Optiprep density centrifugation (Van Deun et

173 al., 2014). Western blot for *P. falciparum* aldolase and exosome marker flotilin-1
174 indicated that EVs were enriched in fractions 7 and 8 (Figure 3A). The density of
175 these fractions was 1.10-1.12 g/ml (Figure 3B), which corresponds to the expected
176 range for exosomes (Tauro et al., 2012). Fractions 7 and 8 from 3D7-WT and 3D7-
177 UpsC^R were pooled and three independent biological replicates were processed for
178 mass spectrometry.

179 Peptides detected by mass spectrometry were searched separately against
180 both human and *P. falciparum* databases and low stringency hits were determined. A
181 total of 178 human proteins and 101 parasite proteins were identified (Table 1 and
182 S1). PfEMP1 could not be reliably identified in these data sets, despite being
183 identified by Western blot analysis. When the label-free quantitative (LFQ) intensity
184 measurements of human and *Plasmodium* proteins were compared to intensities of
185 proteins from the Maxquant contaminant database, *Plasmodium* proteins were
186 predominately of lower abundance while contaminant proteins (e.g. serum albumin)
187 dominated higher abundance proteins (Figure S1). As a result, vesicle proteins were
188 less likely to be sampled for MS/MS and more likely to be below detection limits,
189 which are the likely explanations for non-detection of PfEMP1. Other parasite
190 proteins of interest that were reliably identified by proteomics include merozoite
191 surface protein 1 (MSP-1), knob-associated histidine-rich protein (KHARP), PfEMP3,
192 and stevor (Table S1). Furthermore, the exosome marker flotilin-1 and *P. falciparum*
193 aldolase, which were detected by Western blot analysis, were reproducibly identified
194 by proteomics.

195 The gene ontology (GO) annotations for proteins were downloaded from
196 UniProt databases for human and *Plasmodium* (Table S2). Similarities in

197 overarching molecular function of human and malaria proteins in iRBC-EVs included
198 'Endopeptidase Activity' and 'ATP Binding' as the most abundant functions in both
199 datasets (Figure 3C). In contrast, proteins with functions in 'Structural Constituent of
200 Ribosomes', 'GTPase Activity', 'Histone Binding', and 'Structural Constituent of
201 Cytoskeleton' were overrepresented in parasites proteins but not human. Moreover,
202 'Serine-type Endopeptidase', 'Heme/Oxygen/Iron Binding', 'Cadherin Binding', and
203 'Receptor Binding' functions were overrepresented in human proteins only.
204 Additionally, the 'Extracellular Exosome' GO annotation for cellular compartment was
205 also enriched in the human protein dataset (Table S2). Network analysis using the
206 STRING database (Szklarczyk et al., 2017) showed protein interactions, and
207 highlighted clusters for 'Proteasome-associated Proteins' for both *Plasmodium* and
208 human data sets (Figure 3D). 'Ribosomal Proteins', 'Rhoptry/Antigen' and
209 'Membrane/Antigen' protein interaction clusters are present for *Plasmodium* proteins,
210 whereas 'Complement/Protease', 'Erythrocyte Membrane', 'Hemoglobin-binding
211 Proteins' and 'Flotillin' clusters are present for human proteins, highlighting functional
212 differences in the two data sets.

213 Quantitative analysis of protein abundance between 3D7-WT and 3D7-UpsC^R
214 iRBC-EVs was performed using LFQ intensities for reproducibly identified proteins
215 via a two-sample t-test. For proteins with a significant p-value (<0.05) the difference
216 between means was also assessed, which demonstrated the majority of statistically
217 significant proteins were not accompanied by large changes in abundance (Table
218 S3, Figure 3E). Of the statistically significant, differentially expressed proteins (Table
219 2), one human protein (Histone H2B) and no parasite proteins found to be above the
220 cut-off log-transformed mean difference of 2. Furthermore, several proteins were
221 reproducibility identified exclusively in one treatment group but were not detected in

222 any replicate of the other, and could not be means tested. Four *Plasmodium* and
223 seven human proteins were detected exclusively in 3D7-UpsC^R iRBC-EVs, whereas
224 two human proteins only detected in 3D7-WT iRBC-EVs (Table S4). These proteins
225 could be of low abundance and below detection limits (Figure S1), or could represent
226 biological differences between groups.

227 **Extracellular vesicles from ring-stage iRBC are less immunostimulatory than** 228 **whole trophozoite iRBC**

229 Mantel et al. (Mantel et al., 2013) reported that CD14⁺ monocytes were the
230 main immune cell population targeted by iRBC-EVs, and that monocyte-derived
231 macrophages stimulated with EVs from late-stage iRBC upregulated the expression
232 of IL-1 β , IL-6, IL-10 and IL-12, and released IL-10 and TNF. However, the response
233 to ring stage iRBC-EVs was not evaluated. We have recently shown that PfEMP1
234 located on the iRBC surface can specifically modulate the monocyte immune
235 response to parasites (Sampaio et al. 2017). However, to investigate whether the
236 presence of PfEMP1 in ring stage iRBC-EVs had a similar effect on monocytes, the
237 optimal EV concentration for cell stimulation was first determined by flow cytometry
238 to achieve the highest response (iRBC-EV) to background (uRBC-EV) signal (Figure
239 S2). The cytokine and chemokine production from primary human monocytes in
240 response to iRBC-EVs from ring-stage 3D7-WT and 3D7-UpsC^R was subsequently
241 assessed. Furthermore, the magnitude of the cytokine response was compared to
242 whole trophozoite-stage iRBC, in order to provide a reference for cytokine responses
243 to known immunostimulatory parasites within the same donor.

244 Primary human monocytes from five donors were co-incubated for 12 hours
245 with 5 μ g/ml of uRBC-EVs or iRBC-EVs from ring-stage 3D7-WT or 3D7-UpsC^R, or

246 intact uRBC or 3D7-WT trophozoite iRBC. Levels of released IL-1 β , IL-6, IL-10, IL-
247 12p40, MCP-1, MIP-1 α , MIP-1 β and TNF, cytokines commonly associated with
248 monocyte responses to malaria (Stanisic et al., 2014), were measured by multiplex
249 cytokine ELISA (Figure 4). As previously observed for human PBMC stimulations
250 with *P. falciparum*, the range of cytokine responses varied from donor to donor
251 (D’Ombrain et al., 2008; Stanisic et al., 2014). Some donors had consistently high
252 cytokine responses to both iRBC-EVs and trophozoites, whereas others did not
253 respond to iRBC-EVs at all (Figure 4). There were significantly more IL-12p40, MCP-
254 1, and MIP-1 β released in response to trophozoites compared to iRBC-EVs, but no
255 differences were seen between stimulation with iRBC-EVs from 3D7-WT versus
256 3D7-UpsC^R parasites. Overall, this data showed that iRBC-EVs from early ring-stage
257 induce low or no cytokine responses from the majority of human donors, but high
258 donor heterogeneity exists.

259 **Ring-stage-derived extracellular vesicles induce transcriptional changes in** 260 **human monocytes that are partially PfEMP1 dependent**

261 Although the monocyte cytokine responses to iRBC-EVs were relatively
262 low, the transcriptional profile of these cells in response to EVs was assessed.
263 Primary human monocytes from six donors were stimulated with EVs from ring-stage
264 3D7-WT, 3D7-UpsC^R, or uRBC for six hours followed by RNA. RNA-sequencing was
265 used to measure transcriptional changes in monocytes in response to EV
266 treatments. Median of 23 million reads (min 16, max 64 million) were obtained for
267 each sample, and >90% of reads were successfully mapped to the human genome.
268 No sequences mapped to the *Plasmodium falciparum* genome. After filtering, 10,123
269 genes were classified as expressed in at least one biological condition as

270 determined by filtering criteria (see methods). A multi-dimensional scaling (MDS) plot
271 shows samples clustering according to stimulation (Figure 5A).

272 Differential expression of genes in monocytes stimulated with uRBC-EVs,
273 3D7-WT iRBC-EVs or 3D7-UpsC^R iRBC-EVs was determined, with a 5% false
274 discovery rate (Figure 5B and C). There were 181 differentially expressed (DE)
275 genes in monocytes stimulated with 3D7-WT iRBC-EV compared to uRBC-EVs,
276 whereas there were 530 DE genes when cells were stimulated with 3D7-UpsC^R
277 iRBC-EVs (Figure 5B, Table 3 and S5). There was no statistically significant
278 difference in gene expression when cells were stimulated with vesicles from 3D7-WT
279 compared to 3D7-UpsC^R. Nevertheless, heatmaps depicting the up- or
280 downregulation of genes in each donor with the different EV stimulations indicated a
281 trend in gene expression changes between monocytes incubated with 3D7-WT and
282 3D7-UpsC^R iRBC-EVs (Figure 5E). This shows that overall gene expression in
283 monocytes following stimulation with iRBC-EVs compared to uRBC-EVs causes
284 significant changes, but that the differences between response to 3D7-WT and to
285 3D7-UpsC^R iRBC-EVs are more subtle. Notably, there were 2.9-fold more DE genes
286 in cells stimulated with 3D7-UpsC^R iRBC-EVs versus 3D7-WT iRBC-EVs, compared
287 to uRBC-EV stimulus, indicating that monocytes had a consistently greater response
288 to 3D7-UpsC^R iRBC-EVs.

289 There was some overlap between the DE genes in monocytes stimulated
290 with iRBC-EVs from 3D7-WT compared to 3D7-UpsC^R (Figure 5D). Of the 181 DE
291 genes in 3D7-WT iRBC-EV treatment, 143 (79%) were also changed in 3D7-UpsC^R.
292 In comparison, only 27% of DE genes in 3D7-UpsC^R iRBC-EV-stimulated were also
293 changed in 3D7-WT iRBC-EV-stimulated cells. However, nearly half of the top

294 twenty most differentially expressed genes in both treatments were the same (Table
295 4). The majority of these common DE genes are involved in transcription/translation,
296 and all were upregulated in both sample sets. As there were minimal changes in
297 protein content of iRBC-EVs from 3D7-WT versus 3D7-UpsC^R, with the exception of
298 PfEMP1, it is possible that differences in monocyte transcriptional changes between
299 the two stimulations were due to PfEMP1 presence/absence.

300 **Pathway analysis of gene expression changes in monocytes treated with** 301 **iRBC-derived extracellular vesicles**

302 In order to characterize the functional differences in the effect of monocyte
303 stimulus with 3D7-WT and 3D7-UpsC^R iRBC-EVs, the GO pathways enriched in
304 each data set were inferred (Table 5 and S6). Of the twenty most highly associated
305 GO terms in the iRBC-EV stimulated samples, ten were common between the two
306 treatments. In addition to transcription/translation processes, there was an
307 enrichment of GO terms related to cellular metabolism/catabolism. Of interest are the
308 enriched GO terms that were not in common between the two treatments. These
309 included 'defense response', 'cellular response to cytokine stimulus', and 'response
310 to stress' enriched only with 3D7-UpsC^R iRBC-EV stimulus, and not with 3D7-WT
311 iRBC-EVs. In addition, there was enrichment of terms involving antigen presentation
312 in both treatment groups.

313 Type I interferons were recently found to be released in response to human
314 malaria infection, but to suppress immunity to the infection (Montes de Oca et al.,
315 2016). To determine if there was an effect on genes specifically associated with
316 interferon response, DE genes were searched against the Interferome database. Of
317 the 181 DE genes induced by 3D7-WT iRBC-EVs, 30 were interferon response

318 genes (16.5%), and of the 530 DE genes induced by 3D7-UpsCR iRBC-EVs, 79
319 were interferon response genes (14.9%). In comparison, of the 10,123 genes in the
320 data set, 1,182 were identified as interferon response genes (11.6%). This suggests
321 that treatment of monocytes with iRBC-EVs could elicit a type I interferon response
322 signature.

323 Discussion

324 Extracellular vesicles are increasingly being recognised to play important
325 roles in parasite cell-cell communication and interaction with the host (Mantel &
326 Marti, 2014; Sampaio et al., 2017). Many parasite species produce EVs and employ
327 these for modulation of host cells, which enhances pathogenesis (Szempruch et al.,
328 2016; Twu et al., 2013) and/or inhibits immune responses (Buck et al., 2014;
329 Silverman et al., 2010). The discovery that *P. falciparum* can use EVs for intra-
330 parasite communication and exchange of genetic information (Mantel et al., 2013;
331 Regev-Rudzki et al., 2013) has revealed a new aspect of parasite biology and
332 potential host interactions. We investigated EVs from early ring-stage iRBC, and
333 found that these vesicles contain PfEMP1 and induce transcriptional changes in
334 human monocytes.

335 PfEMP1 is a transmembrane protein that is a key virulence factor in *P.*
336 *falciparum* malaria, largely responsible for the enhanced pathogenesis and mortality
337 associated with this disease (Miller, Baruch, Marsh, & Doumbo, 2002). We
338 demonstrated that PfEMP1 is present in a novel parasite compartment, and may
339 affect the host response to infection. The protein content of *P. falciparum* iRBC-EVs
340 differed throughout the parasite life cycle, notably with the presence of PfEMP1 in
341 EVs released only from early ring-stage iRBC. Of note, the limited timeframe in

342 which PfEMP1 was observed in EVs was different from the appearance of PfEMP1
343 at the iRBC plasma membrane. PfEMP1 trafficking occurs through intracellular
344 vesicles moving from the parasite to the cell membrane, via the Maurer's clefts,
345 (McMillan et al., 2013). It is conceivable that the PfEMP1-containing EVs studied
346 here were released as a byproduct of PfEMP1 transport to the RBC surface.
347 However, PfEMP1 is only present in EVs in the first 12 hours post-invasion, whereas
348 the intracellular transport of PfEMP1 still occurs after 12 hours, indicating the
349 processes are temporally distinct. Therefore, it is unlikely that the intracellular
350 PfEMP1-trafficking vesicles correspond to the EVs studied here. This suggests that
351 the inclusion of PfEMP1 in EVs could be a specific mechanism applied by the
352 parasite to affect host cells.

353 EVs from late-stage iRBC contain miRNA that can downregulate target genes
354 in endothelial cells to affect barrier function (Mantel et al., 2016). Since PfEMP1 can
355 interact with a variety of host cell receptors and dampen cytokine responses from
356 innate immune cells, it is possible that delivery of PfEMP1 via EVs could provide an
357 additional means of host manipulation. Alternatively, PfEMP1 could be deployed in
358 EVs early during parasite infection as a decoy antigen. Indeed, *Trypanosoma cruzi*
359 employ EVs as a decoy for complement attack (Cestari, Ansa-Addo, Deolindo, Inal,
360 & Ramirez, 2012; Díaz Lozano et al., 2017), and exosomes have also been
361 implicated in evasion of humoral immunity in cancer (Aung et al., 2011). A significant
362 proportion of the natural antibody immunity against *P. falciparum* targets PfEMP1
363 (Bull et al., 1998), and *P. falciparum* EVs can be detected by serum from malaria-
364 infected patients *in vitro* (Mantel et al., 2013). Hence, PfEMP1-containing EVs could
365 serve to attract neutralizing antibodies to protect the parasite against targeted

366 immune attack. It would be interesting to evaluate whether parasite EVs from
367 malaria-infected patients bind parasite-specific antibodies *in vivo*.

368 Although we did not directly investigate the origin of iRBC-EVs, these vesicles
369 were enriched for the exosome marker flotilin-1, and proteins detected in iRBC-EVs
370 by proteomics were highly associated with the exosomal cell compartment according
371 to gene ontology analysis. This suggests that these iRBC-EVs could be exosomes,
372 or at least originate from within the parasite, rather than being microvesicles shed
373 from the iRBC plasma membrane. This is further supported by use of PfEMP1
374 transport knockout parasites, which express PfEMP1, but lack PfEMP1 on the iRBC
375 surface (Maier et al., 2007; Maier et al., 2008). PfEMP1 was present in iRBC-EVs
376 from these knockout parasites indicating that iRBC-EVs originated from the
377 intracellular parasite and were released through a still unknown mechanism.
378 Moreover, another study of *P. falciparum*-derived microparticle/microvesicles, which
379 are large vesicles derived from the iRBC plasma membrane, showed that these
380 contain the parasite ring-infected erythrocyte surface antigen (RESA), which we did
381 not detect in our iRBC-EVs (Nantakomol et al., 2011), further distinguishing them
382 from the more widely investigated surface-derived microparticles. Further studies are
383 needed to determine whether the iRBC-EVs are exosomes, or
384 microvesicles/microparticles from the parasite plasma membrane or from parasite-
385 derived RBC organelles such as Maurer's Clefts.

386 Mass spectrometry of iRBC-EVs from 3D7-WT and 3D7-UpsC^R parasites
387 provided the first in-depth analysis of the protein content of ring-stage iRBC-EVs.
388 Using this method, we detected more peptides than previous proteomic analysis of
389 *P. falciparum* iRBC-EVs (Mantel et al., 2013). In addition, label-free quantitative

390 proteomics provided an unbiased comparison of the protein abundance between
391 3D7-WT and 3D7-UpsC^R vesicles. Overall, there was little difference in the quantity
392 of proteins in iRBC-EVs from both strains, though it is possible that differences in low
393 abundance proteins were not detected by proteomics. Technologies to deplete
394 contaminating proteins from the sample could allow better resolution of lower
395 abundance parasite proteins. There were similarities between the protein content
396 detected in early-stage iRBC-EVs and that reported for late-stage iRBC-EVs (Mantel
397 et al., 2013). Parasite proteins MSP-1, Rhop2, HSP-70, GAPDH, CLAG3.1, Ef1-
398 alpha were among the top twenty proteins identified in both studies, consistent with
399 their expression patterns throughout the parasite life cycle (Llinás, Bozdech, Wong,
400 Adai, & DeRisi, 2006). PfEMP1 was not reported in EVs from trophozoites/schizonts
401 (Mantel et al., 2013), in agreement with our finding that PfEMP1 is only present in
402 early ring-stage iRBC-EVs. The function of the various parasite proteins identified in
403 iRBC-EVs is still largely unknown, and thus further investigations are needed to
404 understand their role in EVs.

405 Human primary monocytes were chosen as the target cell population for
406 investigation of early-stage iRBC EV effects, since these were the primary
407 responders to EVs from late-stage iRBC (Mantel et al., 2013). Although ring-stage
408 iRBC-EVs were less stimulatory than intact trophozoite iRBC, there was still a
409 cytokine response to iRBC-EVs. The main pro-inflammatory agonists from iRBC that
410 are detected by monocytes are GPI and hemozoin, which stimulate TLRs and
411 inflammasomes (Eriksson, Sampaio, & Schofield, 2013; Gazzinelli, Kalantari,
412 Fitzgerald, & Golenbock, 2014). The presence of GPI in iRBC-EVs has not been
413 investigated, but given that many parasite proteins are GPI-anchored (e.g. MSP-1) it
414 is plausible that GPI is present in iRBC-EVs. Moreover, there were high peptide

415 counts from heat shock proteins (Hsp) in our proteomic analysis of ring-stage iRBC-
416 EVs. Hsp are important in parasite survival and adaptation to hostile environments,
417 and are exported to the iRBC cytoplasm during infection (Shonhai, Boshoff, & Blatch,
418 2007). Indeed, Hsp70 is a danger signal known to be enriched in EVs from other
419 species (De Maio, 2011), and Hsp70 in EVs can activate innate immune cells
420 (Gastpar et al., 2005; Lv et al., 2012; Vega et al., 2008). The heat shock proteins in
421 iRBC-EVs could be detected as danger signals, and thus induce monocyte
422 activation. Conversely, EVs used in this work did not contain hemozoin, as this was
423 removed during the EV isolation process. The lack of proinflammatory hemozoin,
424 and the overall lower quantities of parasite agonists, supports the observed low
425 capacity of ring-stage iRBC-EVs to stimulate innate immunity. Thus, these EVs may
426 predominantly provide the parasite with a means of cell-cell communication that has
427 minimal interference from host immune cells. It is important to note, however, that
428 some donors were able to respond to iRBC-EVs, indicating that natural variations in
429 human innate responses likely play a role in detection of ring-stage iRBC-EVs.

430 By using transcriptomics to study monocyte gene expression changes in
431 response to ring-stage iRBC-EVs, we further dissected the effect of these vesicles
432 on human monocytes and the contribution of PfEMP1 in this response. The transfer
433 of antigens from extracellular vesicles to antigen presenting cells for T cell priming
434 has been extensively demonstrated (Beauvillain, Ruiz, Guiton, Bout, & Dimier-
435 Poisson, 2007; Robbins & Morelli, 2014). The upregulation of antigen presentation
436 pathways after stimulation with iRBC-EVs indicates that monocytes can not only
437 sense these EVs but also take up antigens for presentation. Additionally, there was
438 an enrichment of interferon response genes among the genes differentially
439 expressed with iRBC-EV treatment, which could be relevant to the recent discovery

440 that type I interferons suppress innate and adaptive immunity to *P. falciparum*
441 infection in humans (Montes de Oca et al., 2016). Nevertheless, there was a
442 difference in monocyte transcriptome changes when cells were stimulated with
443 PfEMP1-positive or PfEMP1-negative iRBC-EVs. Namely, stimulus with PfEMP1-
444 negative iRBC-EVs induced nearly three-fold more gene expression changes
445 compared to PfEMP1-positive iRBC-EVs, and upregulated pathways involving
446 'defence response', 'cellular response to cytokine stimulus', and 'response to stress',
447 which were not upregulated with the PfEMP1-positive iRBC-EVs. PfEMP1, when in
448 the biologically relevant concentrations and cellular localization of the iRBC surface,
449 inhibits monocyte responses (Sampaio et al. 2017). It is possible that PfEMP1 could
450 also exert an immune modulatory effect on monocytes when delivered via EVs.
451 Hence, PfEMP1 might not affect EV uptake by monocytes, but could potentially
452 manipulate monocyte responses to stimulus, as is seen with PfEMP1 on the iRBC
453 surface. However, further work is still required to unequivocally demonstrate this
454 effect.

455 Recent reports have shown that EVs from late-stage iRBC contain RNA.
456 Since ring-stage iRBC-EVs can provide a means of exchange of genetic material,
457 then these vesicles must also contain nucleic acids. Therefore, nucleic acids in ring-
458 stage iRBC-EVs could also account for transcriptional changes in monocytes.
459 Although we did not detect parasite RNA in monocytes treated with iRBC-EVs, it is
460 possible that parasite nucleic acids were delivered to host cells but degraded prior to
461 RNA extraction. Studies into the nucleic acid content of ring-stage iRBC-EVs, and
462 their effects on host cells, are needed in order for the function of these vesicles to be
463 completely understood.

464 The work presented here demonstrates that EVs from early-stage *P.*
465 *falciparum*-infected RBC affect host monocytes, modifying gene expression while
466 inducing low cytokine secretion. As there have been numerous examples that
467 pathogen-derived EVs can modulate host cells in order to inhibit the immune
468 response and promote pathogen survival, *P. falciparum* might employ EVs for similar
469 outcomes. These findings could have important implications for our understanding of
470 parasite modulation of host immunity, and warrant further investigation into the
471 breadth and magnitude of their effects.

472

473 **Materials and Methods**

474 **Parasite culturing**

475 Reagents were purchased from Sigma-Aldrich unless otherwise specified.
476 Parasites were maintained in RPMI-1640 medium pH 7.4, 25 mg/ml HEPES, 50
477 µg/ml hypoxanthine, 2 mg/ml sodium bicarbonate, 20 µg/ml gentamycin,
478 supplemented with 5% human serum and 0.25% AlbumaxII. Parasites were grown in
479 pooled donor red blood cells (RBC;) provided by the Australian Red Cross at 4%
480 hematocrit, and incubated at 37°C in 1% O₂, 4% CO₂ and 95% N₂. Wild type
481 parasite strains used were 3D7 and CS2. PfEMP1 knockdown 3D7-UpsC^R (Voss et
482 al., 2006), and CS2 parasites with the disrupted SBP-1 (PF3D7_0501300), PTP-1
483 (PF3D7_0202200, PFB0106), and PTP-2 (PF3D7_0731100, MAL7P1.172) genes,
484 referred to respectively as CS2-SBP1-KO, CS2-PTP1-KO, and CS2-PTP2-KO, were
485 kindly provided by Alan Cowman (Maier et al., 2007; Maier et al., 2008). 3D7-UpsC^R
486 parasites cultured in the presence of 4 mg/ml blasticidin-S and 4 nM WR99210, do

487 not express PfEMP1 (Voss et al., 2006). Cultures were routinely screened for
488 mycoplasma contamination using MycoAlert Plus Kit (Lonza).

489 Knob-expressing parasites were selected for by gelatin flotation fortnightly
490 (Goodyer, Johnson, Eisenthal, & Hayes, 1994). Parasite cultures were synchronized
491 by treating ring-stage parasites with 5% sorbitol solution at 37°C for 10 min to lyse
492 trophozoite/schizont-stage parasites. For tight synchronization, parasites were grown
493 until schizont stage, magnet purified by cell sorting on CS columns (Miltenyi Biotec),
494 and added to fresh uRBC in culture medium for up to 4 hr to allow invasion, then
495 remaining trophozoites/schizonts were lysed using 5% sorbitol (McMillan et al.,
496 2013). For cell stimulations, magnetic cell sorted iRBC were used.

497 **Isolation of iRBC vesicles**

498 Parasites or uRBC were grown in 0.5% AlbumaxII for 12 hr, unless otherwise
499 indicated, and culture medium was collected for vesicle isolation. Vesicles were
500 isolated as described previously (Lässer, Eldh, & Lötvall, 2012). Briefly, cells and
501 cellular debris (e.g. hemozoin) were removed by sequential centrifugation at 300 x g
502 for 5 min, and 3000 x g for 10 min. Large vesicles, cellular organelles, and debris
503 were further removed by passing supernatant through 0.2 µm filter (Sartsted).
504 Vesicles were pelleted by ultracentrifugation in H₂O₂-treated Optiseal tubes
505 (Beckman Coulter) at 120,000 x g overnight at 4°C in a Ti70 rotor, re-suspended in
506 25 ml of PBS and ultracentrifuged at 120,000 x g for 4 hr at 4°C. Vesicle pellets were
507 re-suspended in 50-100 µl of PBS and maintained on ice, or stored at -80°C. A flow
508 chart of vesicle preparation and usage is show in Figure S3. For cell stimulation
509 assays, freshly isolated vesicles were used. Protein concentrations were determined
510 using BCA assay (Pierce) according to manufacturer's instructions.

511 **SDS-PAGE and Western Blotting**

512 Samples were solubilized with NuPAGE LDS sample buffer, reduced with 2-
513 mercaptoethanol, and analyzed on 3-8% Tris-Acetate gels (for PfEMP1 visualization)
514 or 4-12% Bis-Tris gels (NuPAGE, Thermo Fisher Scientific) and transferred to
515 nitrocellulose (Criterion, Bio-Rad) according to manufacturer's instructions.
516 Membranes were blocked with 5% BSA, 0.05% NP-40 Tris-buffered saline (TBS)
517 and probed with anti-Pf Aldolase (Baum et al., 2006), anti-PfEMP1-ATS (clone
518 1B/98-6H1-1), anti-Plasmepsin V (Boddey et al., 2010), anti-Pf ADF1/cofilin (Wong
519 et al., 2011), anti-SR1/sorcin (Abcam), or anti-flotillin (BD biosciences), and HRP-
520 conjugated anti-mouse or anti-Rabbit IgG antibody (Cell Signaling Technology) in
521 0.5% milk, 0.05% NP-40 TBS.

522 **Proteomics**

523 Culture medium from early ring-stage parasites cultured for 12 hr (40 ml, 4%
524 haematocrit, 8% parasitemia) was centrifuged at 3000 x g for 10 min and filtered
525 through a 0.2 µm syringe filter. Samples were concentrated to 1 ml by centrifugal
526 filtration using Vivaspin 20 Polyethersulfone 100,000 MWCO tubes (Sartorius) and
527 fractionated by density using discontinuous Optiprep gradients (Van Deun et al.,
528 2014). Columns were centrifuged in SW40Ti rotor at 100,000 x g for 18 hr at 4°C.
529 Twelve 1 ml fractions were collected and density of fractions was measured using a
530 refractometer (Metler Toedo). Fractions were diluted in PBS, and centrifuged in 70 Ti
531 rotor at 120,000 x g for 4 hr. Pellets were re-suspended using NuPAGE LDS sample
532 buffer, and stored at -20°C.

533 EV protein was solubilized in 2.5% SDS in 100mM Tris (pH 8), reduced with
534 10mM DTT followed by alkylation with 15mM IAM. Proteins were precipitated by
535 methanol-chloroform (Wessel & Flügge, 1984), re-solubilized in 8M Urea in 100mM
536 Tris (pH 8) and protein concentration equalized across samples (BCA assay;
537 Pierce). Protein was digested overnight with Trypsin (Promega) at 37°C (1µg
538 enzyme to 100µg protein). Samples were acidified with 1% trifluoroacetic acid and
539 desalted using solid phase extraction (SPE) with tips packed with styrene divinyl
540 benzene (3M Empore), and fractionated into three fractions as described
541 (Rappsilber, Mann, & Ishihama, 2007). Extracts were dried by vacuum
542 centrifugation, and reconstituted in 2% acetonitrile, 0.1% trifluoroacetic acid for
543 nanoflow liquid chromatography tandem mass spectrometry (Nano LC-MS/MS).

544 Samples were analysed by LC-MS/MS using Orbitrap Lumos mass
545 spectrometer (Thermo Scientific) fitted with nanoflow reversed-phase-HPLC
546 (Ultimate 3000 RSLC, Dionex). The nano-LC system had an Acclaim Pepmap nano-
547 trap column and Pepmap RSLC analytical column (Dionex – C18, 100 Å, 75 µm × 2
548 cm and 75 µm × 50 cm, respectively). 1 µL of the peptide mix was loaded at an
549 isocratic flow of 5 µL/min of 3% CH₃CN containing 0.1% formic acid for 6 min before
550 the enrichment column was switched in-line with the analytical column. The eluents
551 used for the LC were 5% DMSO/0.1% v/v formic acid (solvent A) and 100%
552 CH₃CN/5% DMSO/0.1% formic acid v/v. The gradient used was 3% B to 22% B for
553 29 min, 22% B to 40% B in 10 min, 40% B to 80% B in 5 min and maintained at 80%
554 B for the final 5 min before equilibration for 10 min at 3% B prior to the next analysis.

555 The mass spectrometer was operated in positive-ionization mode (spray
556 voltage 1.9 kV, source temperature 275°C). Lockmass of 401.92272 from DMSO

557 was used. Data-dependent acquisition mode MS spectra scanning from m/z 350-
558 1550 at 120000 resolution with AGC target of $5e^5$ was used. The “top speed”
559 acquisition method mode (3 sec cycle time) on the most intense precursor was used
560 whereby peptide ions with charge states $\geq 2-5$ were isolated with isolation window of
561 1.6 m/z and fragmented with high energy collision (HCD) mode with stepped collision
562 energy of $30 \pm 5\%$. Fragment ion spectra were acquired in Orbitrap at 15000
563 resolution. Dynamic exclusion was activated for 30s.

564 Database searching was performed using MaxQuant (version 1.5.5.1) for
565 label-free quantification (LFQ) (Cox & Mann, 2008; Tyanova, Temu, & Cox, 2016),
566 using the PlasmoDB 3D7 protein coding sequence file (Aurrecochea et al., 2009)
567 for parasite proteins, and human proteins were searched against reviewed protein
568 entries from UniProt. Default parameters were used for target and decoy searching
569 with a false discovery rate (FDR) of 1% imposed for peptide-to-spectrum matches,
570 and the LFQ minimum ratio count set to 1 and matching between runs set to ‘match
571 from and to’. Oxidation of methionine and N-acetylation of proteins’ N-termini were
572 set to variable modifications and carbidomethylation of cysteine was considered
573 fixed modification. The Maxquant output file was imported in Perseus (Tyanova,
574 Temu, Sinitcyn, et al., 2016) (version 1.5.5.3) and proteins/protein groups identified
575 in the reverse database, contaminant database or only by site were removed. Low
576 stringency proteins were filtered to detection in a minimum of three replicates across
577 the six replicates of both treatment groups. For statistical analyses, high stringency
578 proteins were filtered to only include those reproducibly identified in all three
579 biological replicates within at least one sample group.

580 Gene ontology (GO) functions were obtained from Uniprot for non-
581 homologous proteins from human and *Plasmodium*, and GO annotations for
582 molecular function were used for further analysis. Network analysis was performed
583 by submitting the UniProt ascensions to the STRING (Search Tool for the Retrieval
584 of Interacting Genes) software (v10.5; <http://string.db.org>) (Szklarczyk et al., 2017).
585 Interaction networks were visualised for proteins with medium confidence (0.4) with
586 network edges based on evidence, with continuous lines for direct interactions and
587 interrupted lines for indirect interactions. Clustering was based on a MCL algorithm
588 inflation default parameter of 3.

589

590 **Flow cytometric optimization of EV concentration for cell stimulation**

591 Cryopreserved human PBMCs from naïve Melbourne donors were stimulated
592 with 1, 5 or 10 µg/ml exosomes for 12 hrs at 37°C in 5% CO₂. Brefeldin A (10 µg/ml;
593 Sigma, St Louis, MO) and GolgiStop (2µM; BD Biosciences, San Jose, CA) were
594 added for the final 8 hrs of incubation. Cells were incubated for 10 min on ice with
595 PBS containing 10mM glucose and 3mM EDTA to detach adherent cells. PBMCs
596 were surface stained in FACS buffer (PBS containing 0.5% bovine serum albumin
597 and 2 mM EDTA) on ice for 30 min with allophycocyanin-Cy7 (APC-Cy7)-conjugated
598 anti-CD14 (clone MΦP9, BD Biosciences). Aqua live/dead amine reactive dye
599 (Invitrogen) was used for dead cell exclusion. Cells were fixed in 2%
600 paraformaldehyde and permeabilized using Permeabilizing solution 2 (BD
601 Biosciences). Intracellular staining with Alexa700-conjugated anti-TNF α (clone
602 MAb11; BD Biosciences), PE-conjugated anti-MIP1 α (clone 93342; RnD Systems,
603 Minneapolis MN) and APC-conjugated anti-MIP1 β (clone 24006; RnD Systems) was

604 performed on ice for 1 hr. Samples were analyzed on a four-laser Fortessa flow
605 cytometer (BD Biosciences). Data analysis was performed using FlowJo software
606 (TreeStar, Ashland, OR) and positive populations were determined by a combination
607 of fluorescence minus one (FMOs) and isotype controls.

608

609 **Isolation of primary human monocytes**

610 For cytokine assays, healthy donors were recruited anonymously through the
611 Volunteer Blood Donor Registry. All subjects provided informed written consent, and
612 were self-reported as being malaria naïve. Samples of 100 ml of whole blood were
613 collected into K₂EDTA Vacutainer tubes (BD Biosciences) and processed within 2 hr
614 of collection. For RNA-seq experiments, buffy packs were obtained from the
615 Australian Red Cross, and processed within 24 hr of collection. The study was
616 approved by the human ethics committee at the Walter and Eliza Hall Institute
617 (project no. 13/06).

618 PBMC were purified from whole blood or buffy packs by Lymphoprep gradient
619 centrifugation (D'Ombrain et al., 2007). Monocytes were enriched using isosmotic
620 Percoll (GE Healthcare) density barrier centrifugation as described (de Almeida,
621 Silva, Barral, & Barral Netto, 2000). Briefly, isosmotic Percoll solution (nine parts
622 Percoll to one part NaCl 1.5 M) was mixed 1: (v/v) with PBS/citrate (NaH₂PO₄ 1.49
623 mM; Na₂HPO₄ 9.15 mM; NaCl 139.97 mM; C₆H₅Na₃O₇ ·2H₂O 13mM; pH 7.2).
624 Freshly isolated PBMC (5 ml at 1-2 x 10⁷ cells/ml in PBS) was overlaid on 9 ml
625 isosmotic Percoll/PBS/citrate solution in 15 ml centrifuge tubes, and centrifuged at
626 400 x g for 35 min. Monocytes at the PBS-Percoll interphase were collected and

627 washed twice with PBS before culturing in medium (RPMI-1640, 2 mM L-glutamine,
628 25 μ M HEPES, 100 U/ml penicillin and 100 μ g/ml streptomycin) supplemented with
629 10% FCS. Monocyte purity was verified by CD14 surface staining (CD14-FITC, clone
630 M5E2; BD) and analysed on a FACS Calibur. Purity was on average ~80% (range
631 75-95%). For RNA-seq experiments, monocytes were further purified by FACS
632 sorting gating on monocytes based on forward and side scatter. After sorting,
633 monocyte purity was \geq 99%.

634 **Monocyte stimulation with parasite-derived vesicles**

635 Tightly synchronized parasites at a minimum of 5% parasitemia, or uRBC
636 control, were incubated at 4% hematocrit in 0.5% Albumax parasite medium for 12 hr
637 prior to supernatant collection and vesicle purification. For uRBC control, fresh uRBC
638 were washed in RPMI-HEPES and incubated at 37°C for 48 hr prior to setting up for
639 vesicle collection. Vesicle preparations were maintained endotoxin-free to exclude
640 potential non-specific responses. Monocytes from naïve Melbourne donors were
641 added to triplicate wells in 96-well U-bottom plates at 2×10^5 cells/well, and
642 stimulated with vesicles (5 μ g/ml), or LPS positive control (3.5 ng/ml), for 12 hr at
643 37°C in 5% CO₂. In some instances, monocytes were also stimulated with 6×10^5
644 cells/well uRBC or iRBC. After incubation, plates were centrifuged and cell-free
645 supernatants were collected and stored at -80°C until ready for use.

646

647 **Multiplex cytokine/chemokine ELISA**

648 Cell culture supernatants from stimulated monocytes (triplicate wells) were
649 pooled and tested in duplicate. Multiplex ELISA (Bio-Plex Pro Assay; Bio-Rad) on a
650 Luminex platform was performed according to manufacturer's instructions.

651 **Library preparation and transcriptome sequencing**

652 Human primary monocytes from 6 donors were isolated and stimulated with
653 vesicles as described above for 6 hr. RNA was extracted using RNeasy Plus Kit
654 (Qiagen) according to manufacturer's instructions. RNA and cDNA were quantified
655 using the Agilent Tapestation and the Qubit DNA BR assay kit for Qubit 3.0
656 Fluorometer (Life technologies). An input of 100 ng of total RNA were prepared and
657 indexed separately for sequencing using the TruSeq RNA sample Prep Kit (Illumina)
658 as per manufacturer's instruction. Each library was quantified, and the indexed
659 libraries were pooled and diluted to 1.5 pM for paired end sequencing on a NextSeq
660 500 generating 75 base pair paired end reads, using the v2 150 cycle High Output kit
661 (Illumina) as per manufacturer's instructions.

662 **Gene expression analysis**

663 All samples were aligned to the human genome (GRCh38) using the
664 Rsubread aligner (Liao, Smyth, & Shi, 2013), where greater than 90% of reads
665 mapped in all samples. The number of fragments overlapping each Entrez gene
666 were summarized using featureCounts (Liao, Smyth, & Shi, 2014) and NCBI RefSeq
667 annotation (ftp://ftp.ncbi.nlm.nih.gov/gene/DATA/GENE_INFO/). Differential
668 expression analyses were undertaken using the edgeR (McCarthy, Chen, & Smyth,
669 2012) and limma (Ritchie et al., 2015) software packages. Any gene which did not
670 achieve a count per million mapped reads (CPM) of 2 in at least 6 samples was

671 deemed to be unexpressed and subsequently filtered from the analysis. Additionally,
672 all genes without current annotation were also removed. Compositional differences
673 between libraries were normalized using the trimmed mean of log expression ratios
674 method (Robinson & Oshlack, 2010). Counts were transformed to log₂-CPM with
675 associated precision weights using voom (Law, Chen, Shi, & Smyth, 2014). Sample
676 specific quality weights were also calculated using limma's arrayWeights function
677 (Liu et al., 2015). Differential expression was assessed using linear models and
678 robust empirical Bayes moderated t-statistics (Phipson, Lee, Majewski, Alexander, &
679 Smyth, 2016). P-values were adjusted to control the false discovery rate (FDR)
680 below 5% using the Benjamini and Hochberg method. To increase precision, the
681 linear models incorporate 4 surrogate variables. These variables adjust the data for
682 two known batch effects – donor and day of sample preparation (Figure S4). They
683 were computed using limma's wsva function with weight.by.sd set to true.

684 Gene ontology (GO) pathway analyses used the limma goana function. To
685 make the heatmap and multi-dimension scaling plot, the expression of each gene
686 was summarised as a log₂-CPM with a prior count of 2. These values were then
687 adjusted using limma's removeBatchEffect function to incorporate the surrogate
688 variable correction. The plots were made with limma's coolmap and plotMDS
689 functions respectively. To reduce redundancy in GO terms, the REVIGO program
690 (Supek, Bošnjak, Škunca, & Šmuc, 2011) was applied.

691 To identify any *Plasmodium falciparum* RNA in the samples, an index was
692 built using the Rsubread package (Liao et al., 2013) that contained both the human
693 and *falciparum* genomes (assemblies GRCh38 and *P. falciparum* 3D7 respectively).
694 All samples were then aligned to the combined genome using the Rsubread aligner.

695 The number of reads aligning to *P. falciparum* chromosomes was quantified using
696 featureCounts from Rsubread.

697

698

699 **Table 1 – Top twenty identified proteins in iRBC vesicle preparations by**
 700 **peptide count**

Protein IDs	Protein name	Unique peptide count
<i>Plasmodium falciparum</i> protein		
PF3D7_0930300.1	Merozoite surface protein 1	22
PF3D7_0929400.1	High molecular weight rhoptry protein 2	19
PF3D7_1357100.1	Elongation factor 1-alpha	17
PF3D7_0302500.1;	Cytoadherence linked asexual protein 3.1; cytoadherence linked	11
PF3D7_0302200.1	asexual protein 3.2	
PF3D7_0818900.1	Heat shock protein 70; heat shock protein 70	11
PF3D7_0915400.1	ATP-dependent 6-phosphofructokinase	11
PF3D7_0727400.1	Proteasome subunit alpha type-5, putative	10
PF3D7_0917900.1	Heat shock protein 70	10
PF3D7_1462800.1	Glyceraldehyde-3-phosphate dehydrogenase	9
PF3D7_0608500.1	Proteasome subunit alpha type-2, putative	8
PF3D7_0708400.1	Heat shock protein 90	7
PF3D7_0922600.1	Glutamine synthetase, putative	7
PF3D7_1117700.1	GTP-binding nuclear protein RAN/TC4	7
PF3D7_1353800.1	Proteasome subunit alpha type-4, putative	7
PF3D7_1470900.1	Proteasome subunit beta type-2, putative	7
PF3D7_0317000.1	Proteasome subunit alpha type-3, putative	6
PF3D7_0803800.1	Proteasome subunit beta type-4	6
PF3D7_0905400.1	High molecular weight rhoptry protein 3	6
PF3D7_1015600.1	Heat shock protein 60	6
PF3D7_1444800.1	Fructose-bisphosphate aldolase	6
Human proteins		
P02549	Spectrin alpha chain, erythrocytic 1	34
P55072	Transitional endoplasmic reticulum ATPase	24
P11277	Spectrin beta chain, erythrocytic	22
P04040	Catalase	18
P16157	Ankyrin-1	17
P01023	Alpha-2-macroglobulin	14
P02730	Band 3 anion transport protein	13
P27105	Erythrocyte band 7 integral membrane protein	12
P01024	Complement C3	11

P13798	Acylamino-acid-releasing enzyme	10
P04075	Fructose-bisphosphate aldolase A	9
P11171	Protein 4.1	9
P04406	Glyceraldehyde-3-phosphate dehydrogenase	8
P13716	Delta-aminolevulinic acid dehydratase	8
P25786	Proteasome subunit alpha type-1	8
P25789	Proteasome subunit alpha type-4	8
P28074	Proteasome subunit beta type-5	8
P60900	Proteasome subunit alpha type-6	8
O14818; Q8TAA3	Proteasome subunit alpha type-7; Proteasome subunit alpha type-7-like	7
P00352	Retinal dehydrogenase 1	7

701

702

703

704 **Table 2 – Proteins quantitatively different between vesicles from 3D7-WT iRBC**
 705 **and vesicles 3D7-UpsC^R iRBC**

Protein IDs	Protein names	Protein/gene acronym	GO annotation	Log Student's T-test p-value	Mean's Difference
<i>Plasmodium falciparum</i> proteins					
PF3D7_0930300.1	Merozoite surface protein 1	MSP-1	Pathogenesis	3.30	1.57
PF3D7_1462800.1	Glyceraldehyde-3-phosphate dehydrogenase	GAPDH	glycolytic process	2.36	1.48
PF3D7_1368100.1	26S proteasome regulatory subunit RPN11, putative	RPN11	Ubiquitin-dependent protein catabolic process	1.62	1.38
PF3D7_0617900.1; PF3D7_0610400.1	Histone H3 variant; histone H3	H3	Chromosome organization	1.44	-1.13
PF3D7_1328100.1	Proteasome subunit beta type-7, putative	--	Ubiquitin-dependent protein catabolic process	1.37	1.51
Human proteins					
P06737	Glycogen phosphorylase, liver form	GYPL	Glucose homeostasis; glycogen metabolic process	1.94	1.50
Q9H4G4	Golgi-associated plant pathogenesis-related protein 1	GLIPR2	Regulation of ERK1 and ERK2 cascade;	1.81	0.60
P02790	Hemopexin	HPX	Cellular iron ion homeostasis;	1.78	-1.49
P00338	L-lactate dehydrogenase A chain	LDHA	Glycolytic process;	1.62	0.27
Q99880; Q99879; Q99877; Q93079; Q8N257; Q5QNW6; Q16778; P62807;	Histone H2B (multiple types)	H2B	DNA binding	1.52	2.91

P58876; P57053; P33778; P23527; P06899; O60814; Q96A08 Q99436	Proteasome subunit beta type-7	PSMB7	Proteasome-mediated ubiquitin-dependent protein catabolic process	1.48	-1.00
P13796; P13797	Plastin-2	LCP1/PLS3	Actin binding	1.44	0.95
	Protein disulfide-isomerase-like protein of the testis		Cell redox homeostasis	1.43	1.65
P16157	Ankyrin-1	ANK1	Cytoskeleton organization	1.42	-0.67
P11166	Solute carrier family 2, facilitated glucose transporter member 1	SLC2A1	Glucose transmembrane transporter activity	1.34	-0.57

706 **GO annotation – main gene ontology biological process terms associated with the protein**

707 **Mean's difference - measure of difference in abundance between means as log-fold change, positive indicating**

708 **increase, negative indicating decrease; cut-off for biologically meaningful difference set at Log-fold 2**

709

710

711 **Table 3. Total number of genes differentially expressed between monocytes**
712 **treated with different vesicle stimulus.**

	WT vs. uRBC	3D7-UpsC ^R vs. uRBC	3D7-UpsC ^R vs. WT
<i>Not significant</i>	9942	9593	10123
<i>Significant</i>	181	530	0
Upregulated	116	326	0
Downregulated	65	204	0

713

714

Author Manuscript

715 **Table 4. Top 20 DE genes in response to 3D7-WT and 3D7-Upsc^R vesicle**
 716 **stimulation, compared to uRBC vesicles**

Gene ID	Symbol	Gene description	Gene type/function	Log FC	Adj. p-value
3D7-WT vs. uRBC					
26118	WSB1	WD repeat and SOCS box containing 1	Ubiquitination	0.43	0.0062
905	CCNT2	cyclin T2	Transcription	0.35	0.0062
22797	TFEC	transcription factor EC	Transcription	0.31	0.0062
6142	RPL18A	ribosomal protein L18a	Translation	-0.37	0.0062
57018	CCNL1	cyclin L1	Translation	0.48	0.0062
6498	SKIL	SKI-like proto-oncogene	Transcription	0.27	0.0062
58487	CREBZF	CREB/ATF bZIP transcription factor	Transcription	0.35	0.0090
6168	RPL37A	ribosomal protein L37a	Translation	-0.23	0.0161
84449	ZNF333	zinc finger protein 333	Transcription	0.38	0.0184
54813	KLHL28	kelch like family member 28	Ubiquitination	0.29	0.0208
22107	ARL5B	ADP ribosylation factor like GTPase 5B	Intracellular signalling	0.28	0.0208
9					
55023	PHIP	pleckstrin homology domain interacting protein	Intracellular signalling	0.32	0.0208
5339	PLEC	plectin	Cellular structure	0.22	0.0208
28546	CRIPAK	cysteine rich PAK1 inhibitor	Intracellular signalling	0.73	0.0208
4					
40248	LINC01000	long intergenic non-protein coding RNA 1000	Non-coding RNA	0.46	0.0249
3					
4637	MYL6	myosin light chain 6	Cell motility	-0.20	0.0249
7072	TIA1	TIA1 cytotoxic granule-associated RNA binding protein	Transcription	0.38	0.0249
72921	LOC72921	uncharacterized LOC729218	Unknown	0.44	0.0249
8	8				
64089	SNX16	sorting nexin 16	Intracellular trafficking	0.32	0.0249
11480	MYSM1	Myb like, SWIRM and MPN domains 1	Transcription	0.33	0.0253
3					
3D7-Upsc ^R vs. uRBC					
58487	CREBZF	CREB/ATF bZIP transcription factor	Transcription	0.56	0.0009
6498	SKIL	SKI-like proto-oncogene	Transcription	0.41	0.0009
26118	WSB1	WD repeat and SOCS box containing 1	Ubiquitination	0.59	0.0009
57018	CCNL1	cyclin L1	Translation	0.69	0.0009

55015	PRPF39	pre-mRNA processing factor 39	Translation	0.66	0.0009
22797	TFEC	transcription factor EC	Transcription	0.41	0.0013
13087	AHSA2	AHA1, activator of heat shock 90kDa protein	Intracellular trafficking	0.98	0.0013
2		ATPase homolog 2 (yeast)			
905	CCNT2	cyclin T2	Transcription	0.46	0.0013
2744	GLS	glutaminase	Metabolism	0.39	0.0016
64089	SNX16	sorting nexin 16	Intracellular trafficking	0.51	0.0016
10061	MIR5047	microRNA 5047	Non-coding RNA	0.90	0.0016
6408					
10011	TMEM170	transmembrane protein 170B	Unknown	0.38	0.0016
3407	B				
7072	TIA1	TIA1 cytotoxic granule-associated RNA binding protein	Transcription	0.59	0.0017
51747	LUC7L3	LUC7 like 3 pre-mRNA splicing factor	Translation	0.65	0.0020
1958	EGR1	early growth response 1	Trancription	-0.99	0.0020
54540	FAM193B	family with sequence similarity 193 member B	Unknown	0.70	0.0020
79982	DNAJB14	DnaJ heat shock protein family (Hsp40) member B14	Intracellular trafficking	0.45	0.0021
54813	KLHL28	kelch like family member 28	Ubiquitination	0.40	0.0022
64859	NABP1	nucleic acid binding protein 1	DNA repair	0.42	0.0022
50999	TMED5	transmembrane p24 trafficking protein 5	Intracellular signaling	0.39	0.0022

717 Genes in blue were enriched by both 3D7-WT and 3D7-UpsC^R EV treatment

718

719

720 **Table 5. Top 20 enriched gene ontology terms enriched in response to 3D7-WT**
 721 **and 3D7-UpsC^R vesicle stimulation, compared to uRBC vesicles**

GO term ID	Description	log10 p-value
3D7-WT vs. uRBC		
GO:0070972	protein localization to endoplasmic reticulum	-18.26
GO:0000184	nuclear-transcribed mRNA catabolic process, nonsense-mediated decay	-16.60
GO:0019083	viral transcription	-15.44
GO:0044033	multi-organism metabolic process	-14.22
GO:0006413	translational initiation	-13.65
GO:0006364	rRNA processing	-12.94
GO:0046700	heterocycle catabolic process	-9.84
GO:0022613	ribonucleoprotein complex biogenesis	-8.99
GO:0061024	membrane organization	-8.63
GO:0034660	ncRNA metabolic process	-7.98
GO:1901566	organonitrogen compound biosynthetic process	-6.72
GO:0051704	multi-organism process	-6.57
GO:0043603	cellular amide metabolic process	-6.43
GO:0016071	mRNA metabolic process	-6.17
GO:1901564	organonitrogen compound metabolic process	-6.08
GO:0042590	antigen processing and presentation of exogenous peptide antigen via MHC class I	-5.49
GO:0009056	catabolic process	-5.41
GO:0006396	RNA processing	-5.11
GO:0044085	cellular component biogenesis	-4.95
GO:1901164	negative regulation of trophoblast cell migration	-4.36
3D7-UpsC ^R vs uRBC		
GO:0070972	protein localization to endoplasmic reticulum	-20.4881
GO:0019058	viral life cycle	-17.2899
GO:0006413	translational initiation	-15.3215
GO:0000184	nuclear-transcribed mRNA catabolic process, nonsense-mediated decay	-14.5452
GO:0046700	heterocycle catabolic process	-10.7375
GO:0006364	rRNA processing	-9.8601
GO:0051704	multi-organism process	-9.4023
GO:0006952	defense response	-9.2865
GO:0048002	antigen processing and presentation of peptide antigen	-8.9586

GO:0043603	cellular amide metabolic process	-7.8297
GO:0019882	antigen processing and presentation	-7.7447
GO:1901566	organonitrogen compound biosynthetic process	-7.4283
GO:0009056	catabolic process	-7.3134
GO:0061024	membrane organization	-7.163
GO:1901564	organonitrogen compound metabolic process	-7.1302
GO:0044763	single-organism cellular process	-7.0565
GO:0022613	ribonucleoprotein complex biogenesis	-6.7282
GO:0042221	response to chemical	-6.6596
GO:0071345	cellular response to cytokine stimulus	-6.3799
GO:0006950	response to stress	-6.3439

722 Terms in blue were enriched by both 3D7-WT and 3D7-UpsC^R EV treatment

723 GO term ID – gene ontology term identification number

724

725

726

727 **Figure 1. Variation in parasite protein content in vesicles from different iRBC**
728 **life stages.** CS2-infected iRBC were tightly synchronized and cell culture
729 supernatants were collected at 0-12 hr, 12-24 hr, 24-36 hr, and 36-48 hr. A) Giemsa
730 stain of parasite cultures at supernatant collection time. B) Lysates from uRBC,
731 trophozoite-stage CS2 iRBC, and CS2 vesicles from culture supernatants collected
732 at the specified time points, were analysed by Western Blot for indicated proteins. C)
733 Lysates from uRBC or CS2 iRBC at the specified time points were analysed by
734 Western blot; arrow indicates PfEMP1 and asterisk indicates cross-reactivity with
735 human spectrin. Representative images of two independent repeats.

736

737 **Figure 2. PfEMP1 in vesicles from PfEMP1 transport knock-out and PfEMP1**
738 **expression knock-out parasite strains.** Lysates from uRBC/iRBC and ring-stage
739 vesicles from PfEMP1 transport knock-out parasites PTP1-KO, PTP2-KO and SBP1-
740 KO (A), and lysates and ring-stage vesicles from uRBC, 3D7-WT and PfEMP1
741 expression knock-out 3D7-UpsC^R (B) were analysed for expression of PfEMP1 and
742 other parasite proteins by Western blot. Arrow indicates PfEMP1 and asterisk
743 indicates cross-reactivity with human spectrin. Representative images of two
744 independent repeats. Representative images of minimum two independent repeats.

745

746 **Figure 3. Proteomic analysis of protein content of vesicles from 3D7-WT and**
747 **3D7-UpsC^R iRBC.** A) Cell culture supernatant from ring-stage 3D7-WT iRBC was
748 fractionated by Optiprep density centrifugation, and fraction pairs were analysed by
749 Western blot for *P. falciparum* aldolase and human exosome marker flotilin-1,

750 compared to unfractionated vesicles. B) Fractions 3-10, prepared as in (A), were
751 analysed by Western blot for flotilin-1, and density of individual fractions was
752 measured. C) Overarching molecular function gene ontologies of low stringency
753 proteins identified by mass spectrometry analysis of vesicles from both 3D7-WT and
754 3D7-UpsC^R ring-stage iRBC, from fractions 7 and 8 of samples fractionated as in
755 (A). Gene ontologies of both *Plasmodium falciparum* proteins (left) and human
756 proteins (right) are shown. D) Protein interactome network for iRBC-EVs proteins
757 identified from *Plasmodium* and human databases using the STRING software.
758 Proteins nodes and interactions (direct/physical and indirect/functional represented
759 by continuous and interrupted lines, respectively) are coloured according to MCL
760 clustering. E) Volcano plots of quantitative analysis of proteins in vesicles from 3D7-
761 WT vs. 3D7-UpsC^R, showing log-fold change t-test difference in the x-axis and log-P-
762 value in the y-axis. Blue horizontal line indicates cut-off for $P=0.05$, and yellow,
763 orange, and red vertical lines indicate means difference log-fold of 1, 1.5, and 2,
764 respectively. Quantitation of both *Plasmodium falciparum* proteins (left) and human
765 proteins (right) are shown. Three biological replicates were used for mass
766 spectrometry analysis in (C) and (D).

767

768 **Figure 4. Monocyte cytokine responses to stimulus with parasite vesicles and**
769 **iRBC.** Naïve primary human monocytes (n=5 donors) were negatively isolated and
770 stimulated for 12 hr with 5 µg/ml of vesicles from uRBC, 3D7-WT or 3D7-UpsC^R
771 iRBC, or whole intact uRBC or 3D7-WT trophozoites (ratio of 3 RBC/iRBC to 1
772 monocyte). Levels of indicated cytokines in the culture supernatant were measured

773 by multiplex cytokine ELISA. Data shown is after subtraction of uRBC background
774 from iRBC-stimulated samples. Two-way ANOVA, * indicates $P < 0.05$.

775

776 **Figure 5. RNA-sequencing of monocytes stimulated with vesicles from uRBC,**
777 **3D7-WT iRBC and 3D7-UpsC^R iRBC.** Naïve primary human monocytes (n=6
778 donors) were negatively isolated and stimulated for 6 hr with 5 µg/ml of vesicles from
779 uRBC, 3D7-WT or 3D7-UpsC^R iRBC, prior to RNA extraction and RNA-sequencing.
780 A) Multi-dimensional scaling plot after correction for donor and experimental day
781 effects. Samples in orange, mauve, and green represent uRBC, 3D7-WT, and 3D7-
782 UpsC^R vesicles stimulated samples, respectively. B) Mean-difference plot of average
783 log-expression for each gene (x-axis) against their log-fold change (y-axis) for 3D7-
784 WT vs. uRBC, C) and 3D7-UpsC^R vs. uRBC. The differentially expressed genes are
785 highlighted, with points coloured in red and blue indicating up- and down-regulated
786 genes respectively. D) Venn diagram of number of up-regulated (red) and down-
787 regulated (blue) genes in common between monocytes stimulated with vesicles from
788 3D7-WT vs. uRBC and 3D7-UpsC^R vs. uRBC. E) Heatmap of the expression of the
789 530 DE genes between 3D7-UpsC^R and uRBC. The Z-scores are batch corrected
790 log-CPM (counts per million) scaled to have mean 0 and standard deviation. Genes
791 are displayed horizontally for each donor (1-6), and stimulus condition (uRBC, 3D7-
792 WT, or 3D7-UpsC^R vesicles) labelled in the bottom. The red and blue colouring
793 indicates increased and decreased expression respectively.

794

795 **Figure S1. Protein abundance rates of human and *Plasmodium* proteins**
796 **compared to contaminant proteins.** Label-free quantitative (LFQ) intensity
797 measurements of human and *Plasmodium* proteins compared to intensities of
798 proteins from the Maxquant contaminant database. Blue bars indicate
799 *Plasmodium* or human proteins and red bars represent contaminant proteins. The x-
800 axis represents *** and the y-axis represents peptide counts. Graphs for individual
801 samples of iRBC-EVs from 3D7-WT or 3D7-UpsC (three replicates each) are shown.

802

803 **Figure S2. Frequency of cytokine-producing CD14+ cells following EV**
804 **stimulation.** PBMCs from naïve donors (n=3) were incubated with 1, 5 or 10 µg/ml
805 of vesicles from uRBC or 3D7-UpsC^R iRBC for 12 hr prior to assessment of TNF,
806 MIP1 α and MIP1 β producing CD14+ cells by flow cytometry. Representative dot plots
807 and summary graphs for each cytokine and for each uRBC-EV and iRBC-EV
808 concentration are presented from one donor.

809

810 **Figure S3. Methodological flow chart depicting sample processing for EV**
811 **isolation.**

812

813 **Figure S4. Multi-dimensional scaling plot shows transcriptomic data clusters**
814 **according to batch effects.** Samples clustered according to day of sample
815 preparation (first plot), and individual donors (second plot).

816

817 **Acknowledgements**

818 We thank Alan Cowman for providing the genetically modified parasite strains. We
819 also thank Justin Boddey for kindly providing the Plasmeprin V antibody and Jake
820 Baum for kindly providing the *Plasmodium falciparum* aldolase and ADF1 antibodies.
821 RNA sequencing was performed at the WEHI Genome Hub with technical assistance
822 from Stephen Wilcox.

823

824 **Funding**

825 This work was supported by National Health and Medical Research Council
826 (NHMRC) grants APP106722 and APP1126395. N.G.S was supported by a NHMRC
827 Dora Lush Scholarship [APP1038030]. This work was made possible through the
828 Victorian State Government Operational Infrastructure Support and Australian
829 Government NHMRC Independent Research Institute Infrastructure Support
830 Scheme.

831

832

833 **References**

- 834 Aung, T., Chapuy, B., Vogel, D., Wenzel, D., Oppermann, M., Lahmann, M., . . .
835 Wulf, G. G. (2011). Exosomal evasion of humoral immunotherapy in
836 aggressive B-cell lymphoma modulated by ATP-binding cassette transporter
837 A3. *Proceedings of the National Academy of Sciences*, 108(37), 15336-
838 15341. doi:10.1073/pnas.1102855108
- 839 Aurrecochea, C., Brestelli, J., Brunk, B. P., Dommer, J., Fischer, S., Gajria, B., . . .
840 Wang, H. (2009). PlasmoDB: a functional genomic database for malaria
841 parasites. *Nucleic Acids Research*, 37, D539-D543. doi:10.1093/nar/gkn814
- 842 Baruch, D. I., Gormely, J. A., Ma, C., Howard, R. J., & Pasloske, B. L. (1996).
843 Plasmodium falciparum erythrocyte membrane protein 1 is a parasitized
844 erythrocyte receptor for adherence to CD36, thrombospondin, and
845 intercellular adhesion molecule 1. *Proceedings of the National Academy of
846 Sciences of the United States of America*, 93(8), 3497-3502.
- 847 Baum, J., Richard, D., Healer, J., Rug, M., Krnajski, Z., Gilberger, T. W., . . .
848 Cowman, A. F. (2006). A conserved molecular motor drives cell invasion and
849 gliding motility across malaria life cycle stages and other apicomplexan
850 parasites. *Journal of Biological Chemistry*, 281(8), 5197-5208. doi:
851 10.1074/jbc.M509807200
- 852 Beauvillain, C., Ruiz, S., Guiton, R., Bout, D., & Dimier-Poisson, I. (2007). A vaccine
853 based on exosomes secreted by a dendritic cell line confers protection
854 against *T. gondii* infection in syngeneic and allogeneic mice. *Microbes and
855 Infection*, 9(14), 1614-1622. doi:10.1016/j.micinf.2007.07.002
- 856 Boddey, J. A., Hodder, A. N., Gunther, S., Gilson, P. R., Patsiouras, H., Kapp, E. A.,
857 . . . Cowman, A. F. (2010). An aspartyl protease directs malaria effector

858 proteins to the host cell. *Nature*, 463(7281), 627-631.
859 doi:10.1038/nature08728

860 Buck, A. H., Coakley, G., Simbari, F., McSorley, H. J., Quintana, J. F., Le Bihan, T., .
861 . . Maizels, R. M. (2014). Exosomes secreted by nematode parasites transfer
862 small RNAs to mammalian cells and modulate innate immunity. *Nature*
863 *Communications*, 5, 5488. doi:10.1038/ncomms6488

864 Bull, P. C., Lowe, B. S., Kortok, M., Molyneux, C. S., Newbold, C. I., & Marsh, K.
865 (1998). Parasite antigens on the infected red cell surface are targets for
866 naturally acquired immunity to malaria. *Nature Medicine*, 4(3), 358-360.

867 Cestari, I., Ansa-Addo, E., Deolindo, P., Inal, J. M., & Ramirez, M. I. (2012).
868 *Trypanosoma cruzi* immune evasion mediated by host cell-derived
869 microvesicles. *The Journal of Immunology*, 188(4), 1942-1952.
870 doi:10.4049/jimmunol.1102053

871 Cooke, B. M., Buckingham, D. W., Glenister, F. K., Fernandez, K. M., Bannister, L.
872 H., Marti, M., . . . Coppel, R. L. (2006). A Maurer's cleft-associated protein is
873 essential for expression of the major malaria virulence antigen on the surface
874 of infected red blood cells. *The Journal of Cell Biology*, 172(6), 899-908.
875 doi:10.1083/jcb.200509122

876 Couper, K. N., Barnes, T., Hafalla, J. C. R., Combes, V., Ryffel, B., Secher, T., . . .
877 de Souza, J. B. (2010). Parasite-derived plasma microparticles contribute
878 significantly to malaria infection-induced inflammation through potent
879 macrophage stimulation. *PLoS Pathogens*, 6(1), e1000744.
880 doi:10.1371/journal.ppat.1000744

881 Cox, J., & Mann, M. (2008). MaxQuant enables high peptide identification rates,
882 individualized p.p.b.-range mass accuracies and proteome-wide protein

883 quantification. *Nature Biotechnology*, 26(12), 1367-1372.
884 doi:10.1038/nbt.1511

885 D'Ombrain, M. C., Robinson, L. J., Stanisic, D. I., Taraika, J., Bernard, N., Michon,
886 P., . . . Schofield, L. (2008). Association of early interferon-gamma production
887 with immunity to clinical malaria: a longitudinal study among Papua New
888 Guinean children. *Clinical Infectious Diseases*, 47(11), 1380-1387.
889 doi:10.1086/592971

890 D'Ombrain, M. C., Voss, T. S., Maier, A. G., Pearce, J. A., Hansen, D. S., Cowman,
891 A. F., & Schofield, L. (2007). Plasmodium falciparum Erythrocyte Membrane
892 Protein-1 Specifically Suppresses Early Production of Host Interferon- γ . *Cell*
893 *Host and Microbe*, 2(2), 130-138. doi:10.1016/j.chom.2007.06.012

894 de Almeida, M. C., Silva, A. C., Barral, A., & Barral Netto, M. (2000). A simple
895 method for human peripheral blood monocyte isolation. *Memórias do Instituto*
896 *Oswaldo Cruz*, 95(2), 221-223.

897 De Maio, A. (2011). Extracellular heat shock proteins, cellular export vesicles, and
898 the Stress Observation System: A form of communication during injury,
899 infection, and cell damage: It is never known how far a controversial finding
900 will go! Dedicated to Ferruccio Ritossa. *Cell Stress & Chaperones*, 16(3), 235-
901 249. doi:10.1007/s12192-010-0236-4

902 Díaz Lozano, I. M., De Pablos, L. M., Longhi, S. A., Zago, M. P., Schijman, A. G., &
903 Osuna, A. (2017). Immune complexes in chronic Chagas disease patients are
904 formed by exovesicles from Trypanosoma cruzi carrying the conserved MASP
905 N-terminal region. *Scientific Reports* 7, 44451. doi:10.1038/srep44451

906 Diaz, S. A., Martin, S. R., Grainger, M., Howell, S. A., Green, J. L., & Holder, A. A.
907 (2014). Plasmodium falciparum aldolase and the C-terminal cytoplasmic

908 domain of certain apical organellar proteins promote actin polymerization.
909 *Molecular and Biochemical Parasitology*, 197(1-2), 9-14.
910 doi:10.1016/j.molbiopara.2014.09.006

911 Eriksson, E. M., Sampaio, N. G., & Schofield, L. (2013). Toll-Like Receptors and
912 Malaria – Sensing and Susceptibility. *Journal of Tropical Diseases*, 2(1), 126-
913 132. doi:10.4172/2329-891X.1000126

914 Gastpar, R., Gehrmann, M., Bausero, M. A., Asea, A., Gross, C., Schroeder, J. A., &
915 Multhoff, G. (2005). Heat shock protein 70 surface-positive tumor exosomes
916 stimulate migratory and cytolytic activity of natural killer cells. *Cancer*
917 *Research*, 65(12), 5238-5247. doi:10.1158/0008-5472.can-04-3804

918 Gazzinelli, R. T., Kalantari, P., Fitzgerald, K. A., & Golenbock, D. T. (2014). Innate
919 sensing of malaria parasites. *Nature Reviews Immunology*, 14(11), 744-757.
920 doi:10.1038/nri3742

921 Goodyer, I. D., Johnson, J., Eisenthal, R., & Hayes, D. J. (1994). Purification of
922 mature-stage Plasmodium falciparum by gelatine flotation. *Annals of Tropical*
923 *Medicine and Parasitology*, 88(2), 209-211.

924 Jensen, A. T. R., Magistrado, P., Sharp, S., Joergensen, L., Lavstsen, T.,
925 Chiucchiuini, A., . . . Theander, T. G. (2004). Plasmodium falciparum
926 associated with severe childhood malaria preferentially expresses PfEMP1
927 encoded by group A var genes. *The Journal of Experimental Medicine*,
928 199(9), 1179-1190. doi:10.1084/jem.20040274

929 Kriek, N., Tilley, L., Horrocks, P., Pinches, R., Elford, B. C., Ferguson, D. J. P., . . .
930 Newbold, C. I. (2003). Characterization of the pathway for transport of the
931 cytoadherence-mediating protein, PfEMP1, to the host cell surface in malaria
932 parasite-infected erythrocytes. *Molecular Microbiology*, 50(4), 1215-1227.

933 Lässer, C., Eldh, M., & Lötval, J. (2012). Isolation and characterization of RNA-
934 containing exosomes. *Journal of visualized experiments* 9(59), e3037.
935 doi:10.3791/3037

936 Law, C. W., Chen, Y., Shi, W., & Smyth, G. K. (2014). Voom: precision weights
937 unlock linear model analysis tools for RNA-seq read counts. *Genome Biology*,
938 15(2), R29. doi:10.1186/gb-2014-15-2-r29

939 Liao, Y., Smyth, G. K., & Shi, W. (2013). The Subread aligner: fast, accurate and
940 scalable read mapping by seed-and-vote. *Nucleic Acids Research*, 41(10),
941 e108-e108. doi:10.1093/nar/gkt214

942 Liao, Y., Smyth, G. K., & Shi, W. (2014). FeatureCounts: an efficient general purpose
943 program for assigning sequence reads to genomic features. *Bioinformatics*,
944 30(7), 923-930. doi:10.1093/bioinformatics/btt656

945 Liu, R., Holik, A. Z., Su, S., Jansz, N., Chen, K., Leong, H. S., . . . Ritchie, M. E.
946 (2015). Why weight? Modelling sample and observational level variability
947 improves power in RNA-seq analyses. *Nucleic Acids Research*, 43(15), e97-
948 e97. doi:10.1093/nar/gkv412

949 Llinás, M., Bozdech, Z., Wong, E. D., Adai, A. T., & DeRisi, J. L. (2006).
950 Comparative whole genome transcriptome analysis of three Plasmodium
951 falciparum strains. *Nucleic Acids Research*, 34(4), 1166-1173.
952 doi:10.1093/nar/gkj517

953 Lv, L.-H., Wan, Y.-L., Lin, Y., Zhang, W., Yang, M., Li, G.-L., . . . Min, J. (2012).
954 Anticancer drugs cause release of exosomes with heat shock proteins from
955 human hepatocellular carcinoma cells that elicit effective natural killer cell
956 antitumor responses in vitro. *Journal of Biological Chemistry*, 287(19), 15874-
957 15885. doi:10.1074/jbc.M112.340588

958 Maier, A. G., Cooke, B. M., Cowman, A. F., & Tilley, L. (2009). Malaria parasite
959 proteins that remodel the host erythrocyte. *Nature Reviews Microbiology*, 7(5),
960 341-354. doi:10.1038/nrmicro2110

961 Maier, A. G., Rug, M., O'Neill, M. T., Beeson, J. G., Marti, M., Reeder, J., &
962 Cowman, A. F. (2007). Skeleton-binding protein 1 functions at the
963 parasitophorous vacuole membrane to traffic PfEMP1 to the Plasmodium
964 falciparum-infected erythrocyte surface. *Blood*, 109(3), 1289-1297.
965 doi:10.1182/blood-2006-08-043364

966 Maier, A. G., Rug, M., O'Neill, M. T., Brown, M., Chakravorty, S., Szestak, T., .
967 . . Cowman, A. F. (2008). Exported proteins required for virulence and rigidity
968 of Plasmodium falciparum-infected human erythrocytes. *Cell*, 134(1), 48-61.
969 doi:10.1016/j.cell.2008.04.051

970 Mantel, P.-Y., Hjelmqvist, D., Walch, M., Kharoubi-Hess, S., Nilsson, S., Ravel, D., . .
971 . Marti, M. (2016). Infected erythrocyte-derived extracellular vesicles alter
972 vascular function via regulatory Ago2-miRNA complexes in malaria. *Nature*
973 *Communications*, 7, 12727. doi:10.1038/ncomms12727

974 Mantel, P.-Y., Hoang, A. N., Goldowitz, I., Potashnikova, D., Hamza, B., Vorobjev, I., .
975 . . . Marti, M. (2013). Malaria-infected erythrocyte-derived microvesicles
976 mediate cellular communication within the parasite population and with the
977 host immune system. *Cell Host and Microbe*, 13(5), 521-534.
978 doi:10.1016/j.chom.2013.04.009

979 Mantel, P.-Y., & Marti, M. (2014). The role of extracellular vesicles in Plasmodium
980 and other protozoan parasites. *Cellular microbiology*, 16(3), 344-354.
981 doi:10.1111/cmi.12259

- 982 Martin-Jaular, L., Nakayasu, E. S., Ferrer, M., Almeida, I. C., & Del Portillo, H. A.
983 (2011). Exosomes from Plasmodium yoelii-infected reticulocytes protect mice
984 from lethal infections. *PloS One*, 6(10), e26588.
985 doi:10.1371/journal.pone.0026588
- 986 McCarthy, D. J., Chen, Y., & Smyth, G. K. (2012). Differential expression analysis of
987 multifactor RNA-Seq experiments with respect to biological variation. *Nucleic
988 Acids Research*, 40(10), 4288-4297. doi:10.1093/nar/gks042
- 989 McMillan, P. J., Millet, C., Batinovic, S., Maiorca, M., Hanssen, E., Kenny, S., . . .
990 Tilley, L. (2013). Spatial and temporal mapping of the PfEMP1 export pathway
991 in Plasmodium falciparum. *Cellular Microbiology*, 15(8), 1401-1418.
992 doi:10.1111/cmi.12125
- 993 Miller, L. H., Baruch, D. I., Marsh, K., & Doumbo, O. K. (2002). The pathogenic basis
994 of malaria. *Nature*, 415(6872), 673-679. doi:10.1038/415673a
- 995 Montes de Oca, M., Kumar, R., Rivera, Fabian de L., Amante, Fiona H., Sheel, M.,
996 Faleiro, Rebecca J., . . . Engwerda, Christian R. (2016). Type I interferons
997 regulate immune responses in humans with blood-stage Plasmodium
998 falciparum infection. *Cell Reports*, 17(2), 399-412.
999 doi:10.1016/j.celrep.2016.09.015
- 1000 Nantakomol, D., Dondorp, A. M., Krudsood, S., Udomsangpetch, R.,
1001 Pattanapanyasat, K., & Combes, V. (2011). Circulating red cell-derived
1002 microparticles in human malaria. *Journal of Infectious Diseases*, 203(5) 700-
1003 706. doi:10.1093/infdis/jiq104
- 1004 Phipson, B., Lee, S., Majewski, I. J., Alexander, W. S., & Smyth, G. K. (2016).
1005 Robust hyperparameter estimation protects against hypervariable genes and

1006 improves power to detect differential expression. *The Annals of Applied*
1007 *Statistics*, 10(2), 946-963. doi:10.1214/16-AOAS920

1008 Rappsilber, J., Mann, M., & Ishihama, Y. (2007). Protocol for micro-purification,
1009 enrichment, pre-fractionation and storage of peptides for proteomics using
1010 StageTips. *Nature Protocols*, 2(8), 1896-1906.

1011 Reeder, J. C., Cowman, A. F., Davern, K. M., Beeson, J. G., Thompson, J. K.,
1012 Rogerson, S. J., & Brown, G. V. (1999). The adhesion of Plasmodium
1013 falciparum-infected erythrocytes to chondroitin sulfate A is mediated by P.
1014 falciparum erythrocyte membrane protein 1. *Proceedings of the National*
1015 *Academy of Sciences*, 96(9), 5198-5202. doi:10.1073/pnas.96.9.5198

1016 Regev-Rudzki, N., Wilson, D. W., Carvalho, T. G., Sisquella, X., Coleman, B. M.,
1017 Rug, M., . . . Cowman, A. F. (2013). Cell-Cell communication between
1018 malaria-infected red blood cells via exosome-like vesicles. *Cell*, 153(5), 1120-
1019 1133. doi:10.1016/j.cell.2013.04.029

1020 Ritchie, M. E., Phipson, B., Wu, D., Hu, Y., Law, C. W., Shi, W., & Smyth, G. K.
1021 (2015). Limma powers differential expression analyses for RNA-sequencing
1022 and microarray studies. *Nucleic Acids Research*, 43(7), e47.
1023 doi:10.1093/nar/gkv007

1024 Robbins, P. D., & Morelli, A. E. (2014). Regulation of immune responses by
1025 extracellular vesicles. *Nature Reviews Immunology*, 14(3), 195-208.
1026 doi:10.1038/nri3622

1027 Robinson, M. D., & Oshlack, A. (2010). A scaling normalization method for
1028 differential expression analysis of RNA-seq data. *Genome Biology*, 11(3),
1029 R25. doi:10.1186/gb-2010-11-3-r25

- 1030 Salzer, U., Hinterdorfer, P., Hunger, U., Borcken, C., & Prohaska, R. (2002). Ca(++)-
1031 dependent vesicle release from erythrocytes involves stomatin-specific lipid
1032 rafts, synexin (annexin VII), and sorcin. *Blood*, 99(7), 2569-2577.
- 1033 Sampaio, N. G., Cheng, L., & Eriksson, E. M. (2017). The role of extracellular
1034 vesicles in malaria biology and pathogenesis. *Malaria Journal*, 16(1), 245.
1035 doi:10.1186/s12936-017-1891-z
- 1036 Sampaio, N. G., Eriksson, E. M., Schofield, L. (2017). *Plasmodium falciparum*
1037 PfEMP1 modulates monocyte/macrophage transcription factor activation, and
1038 cytokine and chemokine responses. *Infection and Immunity*.
1039 doi:10.1128/IAI.00447-17
- 1040 Schofield, L., & Grau, G. E. (2005). Immunological processes in malaria
1041 pathogenesis. *Nature Reviews Immunology*, 5(9), 722-735.
1042 doi:10.1038/nri1686
- 1043 Shonhai, A., Boshoff, A., & Blatch, G. L. (2007). The structural and functional
1044 diversity of Hsp70 proteins from *Plasmodium falciparum*. *Protein Science*,
1045 16(9), 1803-1818. doi:10.1110/ps.072918107
- 1046 Silverman, J. M., Clos, J., Horakova, E., Wang, A. Y., Wiesgigl, M., Kelly, I., . . .
1047 Reiner, N. E. (2010). Leishmania exosomes modulate innate and adaptive
1048 immune responses through effects on monocytes and dendritic cells. *The*
1049 *Journal of Immunology*, 185(9), 5011-5022. doi:10.4049/jimmunol.1000541
- 1050 Stanistic, D. I., Cutts, J., Eriksson, E., Fowkes, F. J. I., Rosanas-Urgell, A., Siba, P., .
1051 . . Schofield, L. (2014). $\gamma\delta$ T cells and CD14+ monocytes are predominant
1052 cellular sources of cytokines and chemokines associated with severe malaria.
1053 *Journal of Infectious Diseases*, 210(2), 295-305. doi:10.1093/infdis/jiu083

- 1054 Supek, F., Bošnjak, M., Škunca, N., & Šmuc, T. (2011). REVIGO summarizes and
1055 visualizes long lists of gene ontology terms. *PloS One*, 6(7), e21800.
1056 doi:10.1371/journal.pone.0021800
- 1057 Szempruch, A. J., Sykes, S. E., Kieft, R., Dennison, L., Becker, A. C., Gartrell, A., . . .
1058 . Harrington, J. M. (2016). Extracellular vesicles from *Trypanosoma brucei*
1059 mediate virulence factor transfer and cause host anemia. *Cell*, 164(1-2), 246-
1060 257. doi:10.1016/j.cell.2015.11.051
- 1061 Szklarczyk, D., Morris, J. H., Cook, H., Kuhn, M., Wyder, S., Simonovic, M., . . .
1062 von Mering, C. (2017). The STRING database in 2017: quality-controlled
1063 protein–protein association networks, made broadly accessible. *Nucleic Acids*
1064 *Research*, 45(Database issue), D362-D368. doi:10.1093/nar/gkw937
- 1065 Tauro, B. J., Greening, D. W., Mathias, R. A., Ji, H., Mathivanan, S., Scott, A. M., &
1066 Simpson, R. J. (2012). Comparison of ultracentrifugation, density gradient
1067 separation, and immunoaffinity capture methods for isolating human colon
1068 cancer cell line LIM1863-derived exosomes. *Methods*, 56(2), 293-304.
1069 doi:10.1016/j.ymeth.2012.01.002
- 1070 Tembo, D. L., Nyoni, B., Murikoli, R. V., Mukaka, M., Milner, D. A., Berriman, M., . . .
1071 Montgomery, J. (2014). Differential PfEMP1 expression is associated with
1072 cerebral malaria pathology. *PLoS Pathogens*, 10(12), e1004537.
1073 doi:10.1371/journal.ppat.1004537
- 1074 Twu, O., de Miguel, N., Lustig, G., Stevens, G. C., Vashisht, A. A., Wohlschlegel, J.
1075 A., & Johnson, P. J. (2013). *Trichomonas vaginalis* exosomes deliver cargo to
1076 host cells and mediate host: parasite interactions. *PLoS Pathogens*, 9(7),
1077 e1003482. doi:10.1371/journal.ppat.1003482

1078 Tyanova, S., Temu, T., & Cox, J. (2016). The MaxQuant computational platform for
1079 mass spectrometry-based shotgun proteomics. *Nature Protocols*, 11(12),
1080 2301-2319. doi:10.1038/nprot.2016.136

1081 Tyanova, S., Temu, T., Sinitcyn, P., Carlson, A., Hein, M. Y., Geiger, T., . . . Cox, J.
1082 (2016). The Perseus computational platform for comprehensive analysis of
1083 (prote)omics data. *Nature Methods*, 13(9), 731-740. doi:10.1038/nmeth.3901

1084 Van Deun, J., Mestdagh, P., Sormunen, R., Cocquyt, V., Vermaelen, K.,
1085 Vandesompele, J., . . . Hendrix, A. (2014). The impact of disparate isolation
1086 methods for extracellular vesicles on downstream RNA profiling. *Journal of*
1087 *Extracellular Vesicles*, 3. doi:10.3402/jev.v3.24858

1088 Vega, V. L., Rodríguez-Silva, M., Frey, T., Gehrmann, M., Diaz, J. C., Steinem, C., . .
1089 . De Maio, A. (2008). Hsp70 translocates into the plasma membrane after
1090 stress and is released into the extracellular environment in a membrane-
1091 associated form that activates macrophages. *The Journal of Immunology*,
1092 180(6), 4299-4307. doi:10.4049/jimmunol.180.6.4299

1093 Voss, T. S., Healer, J., Marty, A. J., Duffy, M. F., Thompson, J. K., Beeson, J. G., . . .
1094 Cowman, A. F. (2006). A var gene promoter controls allelic exclusion of
1095 virulence genes in Plasmodium falciparum malaria. *Nature*, 439(7079), 1004-
1096 1008. doi:10.1038/nature04407

1097 Wessel, D., & Flügge, U. I. (1984). A method for the quantitative recovery of protein
1098 in dilute solution in the presence of detergents and lipids. *Analytical*
1099 *Biochemistry*, 138(1), 141-143.

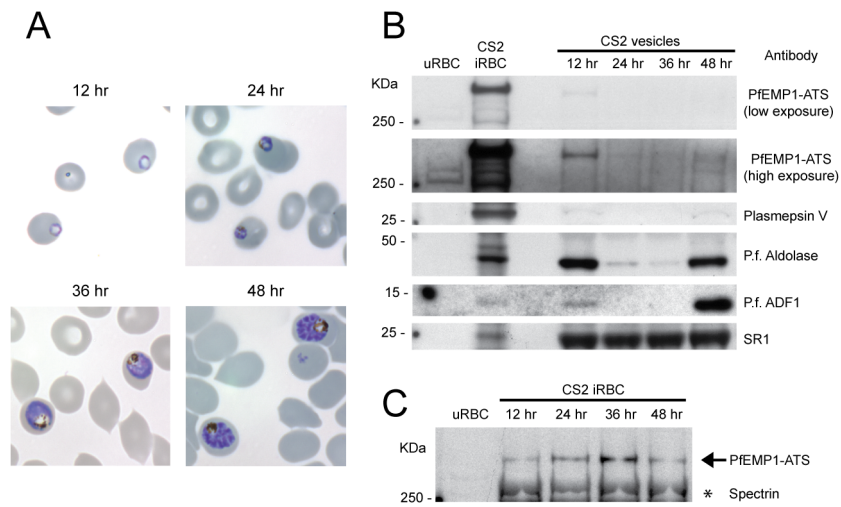
1100 White, N. J., Pukrittayakamee, S., Hien, T. T., Faiz, M. A., Mokuolu, O. A., &
1101 Dondorp, A. M. (2014). Malaria. *The Lancet*, 383(9918), 723-735.
1102 doi:10.1016/S0140-6736(13)60024-0

1103 Wong, W., Skau, C. T., Marapana, D. S., Hanssen, E., Taylor, N. L., Riglar, D. T., . .
1104 . Baum, J. (2011). Minimal requirements for actin filament disassembly
1105 revealed by structural analysis of malaria parasite actin-depolymerizing factor
1106 1. *Proceedings of the National Academy of Sciences*, 108(24), 9869-9874.
1107 doi:10.1073/pnas.1018927108

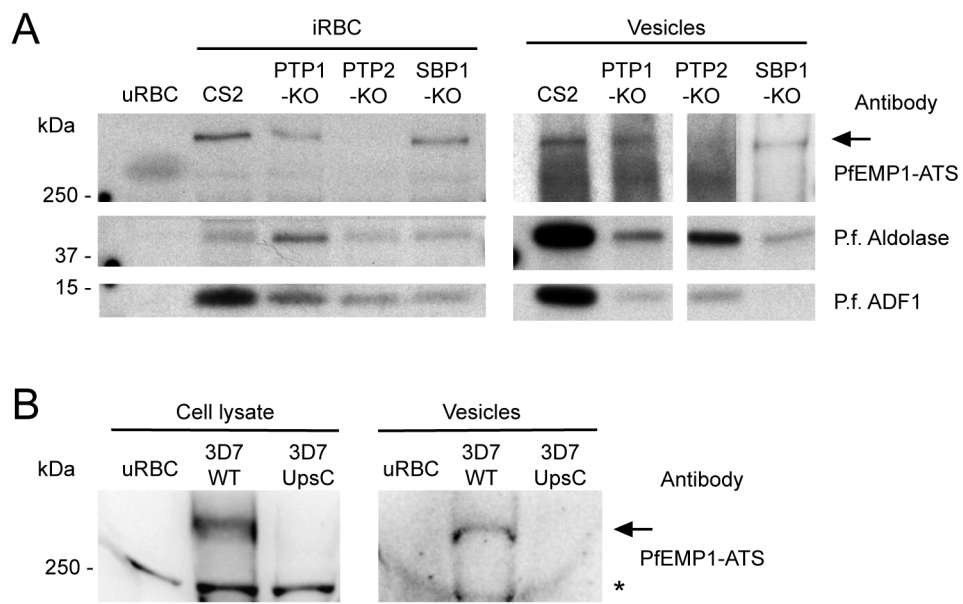
1108 Wong, W., Webb, A. I., Olshina, M. A., Infusini, G., Tan, Y. H., Hanssen, E., . . .
1109 Baum, J. (2014). A mechanism for actin filament severing by malaria parasite
1110 actin depolymerizing factor 1 via a low affinity binding interface. *Journal of*
1111 *Biological Chemistry*, 289(7), 4043-4054. doi:10.1074/jbc.M113.523365

1112

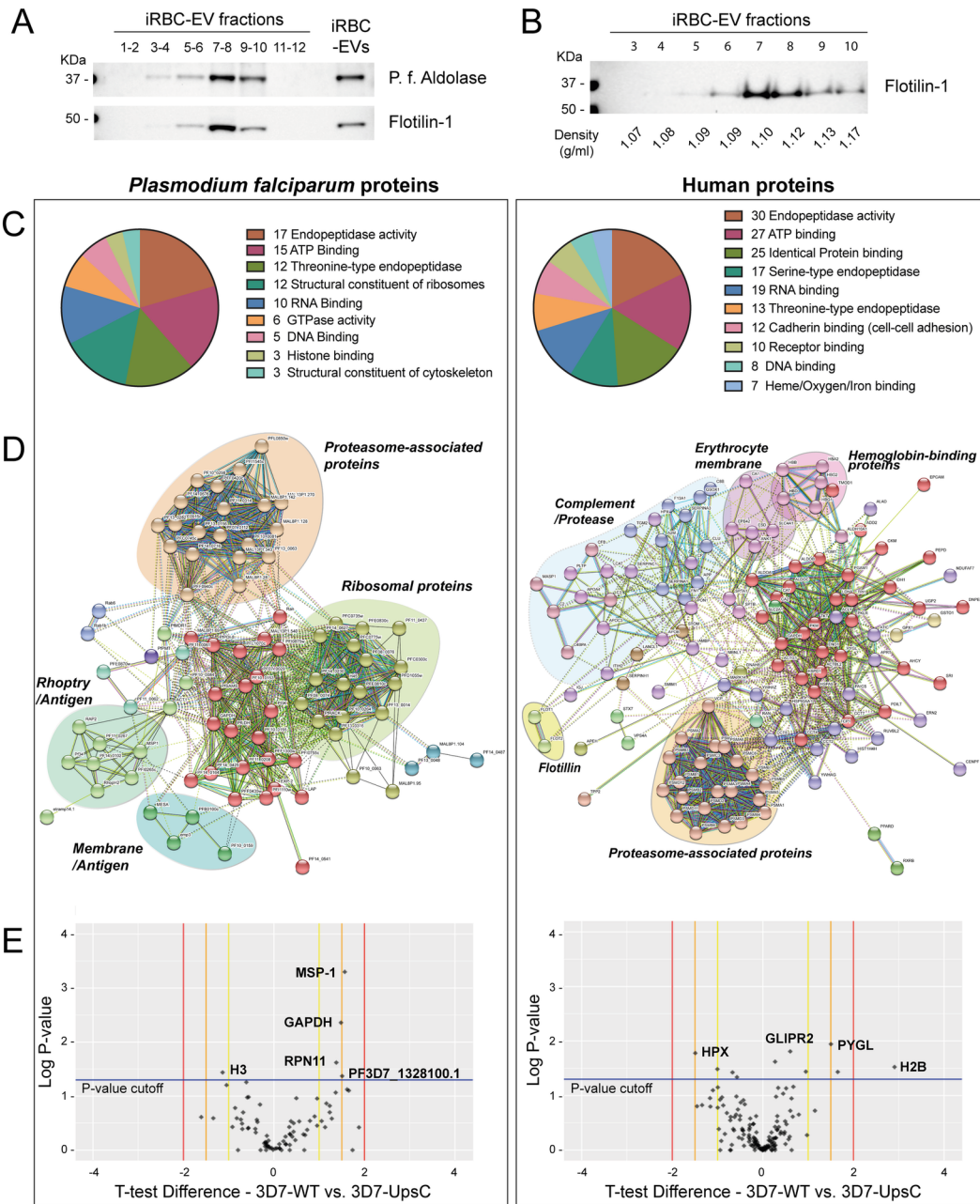
1113



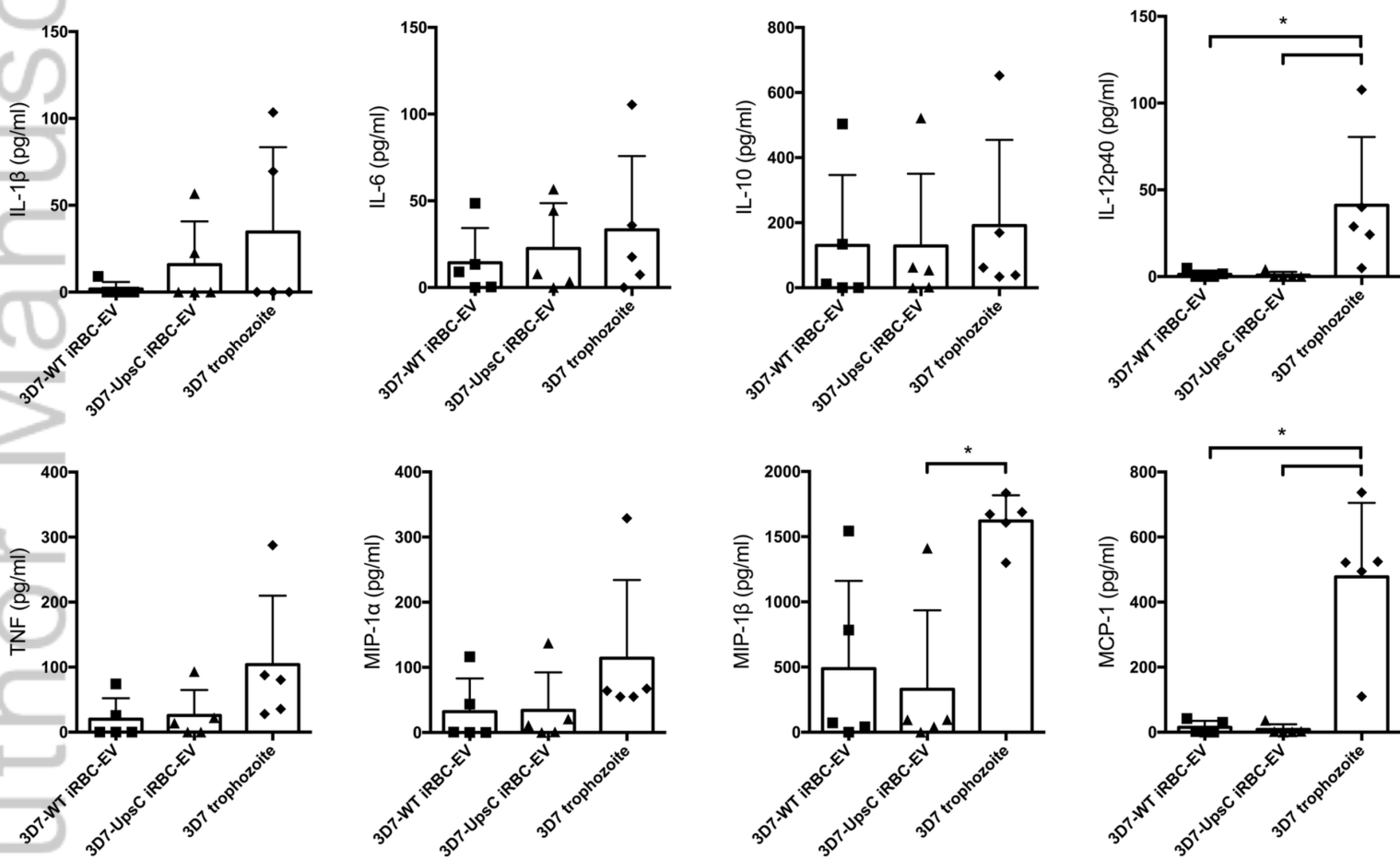
CMI_12822_F1.tif



CMI_12822_F2.tiff



CMI_12822_F3.tif



CMI_12822_F4.tif

